Available online at www.sciencedirect.com
SCIENCE DIRECT®
ELSEVIER
International Journal of Solids and Structures 43 (2006) 497–522
INTERNATIONAL JOURNAL OF SOLIDS and STRUCTURES
www.elsevier.com/locate/ijsolstr

On the longitudinal impact of two phase transforming bars. Elastic versus a rate-type approach. Part I: The elastic case

Cristian Făciu [a,*], Alain Molinari [b]

[a] *Institute of Mathematics of the Romanian Academy, P.O. Box 1-764, RO-014700 Bucharest, Romania*
[b] *Laboratoire de Physique et Mécanique des Matériaux, UMR—CNRS 7554, Université de Metz, Ile du Saulcy, F-57045 Metz, France*

Received 20 September 2004; received in revised form 6 June 2005
Available online 13 September 2005

Abstract

Longitudinal impact experiments of thin bars are proposed as an effective mean for understanding the kinetics of stress-induced phase transformations. We consider on one side the elastic model and on the other side an augmented theory, which includes the Maxwellian rate-type viscoelasticity with finite instantaneous response and as a limiting case the Kelvin–Voigt viscoelasticity with infinite instantaneous response. By using the chord criterion, we investigate the complete set of Goursat and Riemann problems which could arise as a result of dynamic interactions when we consider a piecewise linear elastic model corresponding to a three phase material. Subsequently we use our Riemann solvers to construct solutions for the longitudinal impact of two elastic phase transforming bars for a variety of impact conditions. We focus on the results which can be measured in laboratory experiments like the time of separation of the two bars after impact, the profile of the particle velocity at the rear end of the target and the stress history at the contact point. In Part II of this paper we continue with a theoretical and numerical comparative analysis on the wave structure predicted by our general rate-type approach for the same impact problem.

Keywords: Phase transition; Bar impact; Shock waves; Riemann problem; Shape memory alloys

1. Introduction

The motivation of this paper arises from the growing recent interest in understanding the dynamical response of materials supporting phase transformation. For instance, shape memory alloys (SMA) have been

* Corresponding author. Fax: +40 21 319 65 05.
E-mail address: cristian.faciu@imar.ro (C. Făciu).

0020-7683/$ - see front matter © 2005 Elsevier Ltd. All rights reserved.
doi:10.1016/j.ijsolstr.2005.06.023

recently considered for dynamic loading applications due to their high energy absorption capabilities. In spite of this interest, the existing experimental works on the dynamic behavior of SMAs is rather limited. One of the well known experimental investigation was done by Escobar and Clifton (1995) by using a shear-plate impact experiment technique to understand the kinetics of martensitic transformation in single crystals of Cu–Al–Ni SMA. Propagating phase boundaries were not observed directly due to their low propagation speed. Instead, their presence was deduced from measurements of the elastic waves at the rear end of the target plate. Only recently, new impact experiments on the wave propagation in a NiTi SMA rod has been performed in a split-Hopkinson bar apparatus by Lagoudas et al. (2003) in order to determine the dynamic stress–strain relationship due to detwinning.

On the other side, both kinetics and dynamics of phase transformations have been recently subjects of intense theoretical studies (see for instance Chen and Lagoudas (2000), Bruno and Vaynblat (2001), Ngan and Truskinovsky (2002) and the literature therein). Since different models describe differently the metastable states, the nucleation of phases and therefore, lead to distinct solutions for Riemann problems, for example, they are only the laboratory experiments which can validate which is the appropriate one.

We propose in this paper, as a mean for investigating the kinetics of stress-induced phase transformations the longitudinal impact of bars, one of the simplest dynamic laboratory test, but rich in information. Indeed, in a single test one can determine: the time of separation between bars after the impact by optical methods, the particle velocity at the rear end of the target bar by a VISAR interferometry system, the stress history at the impacted end by piezoelectric wafers, the variation in time of the strain at various cross-section by using diffraction gratings. The correlation of such measurements allow a better understanding of the kinetics of transformation. Such kind of experiments have been intensively used a few decades ago in dynamic plasticity (Bell, 1968; Cristescu and Suliciu, 1982).

The purpose of this paper is to start a complete and comparative theoretical and numerical study of the predictions of one of the simplest constitutive laws for SMAs, the elastic non-monotone model and its Maxwellian rate-type dissipative regularization, when we consider longitudinal impact loading conditions.

Inaugurated by Ericksen (1975) for the static case and by James (1980) for the dynamic case, studies of elastic bar theory have indicated that the main features of phase transitions in a two-phase material are predicted by the use of a non-convex stored energy, or, equivalently a non-monotone stress–strain relation. Physically, the non-convexity of elastic energy reflects the bi-stability of the constitutive elements. This approach has been extended for the 3-D case (see for instance James, 1981) and there is now a vast literature on this subject. The usual continuum theory of elasticity, though adequate for characterizing two-phase energy minimizers, does not, by itself, characterize quasi-static or dynamic *processes* of a body involving transitions from one phase to another. This is illustrated by the tremendous lack of uniqueness of solution to particular initial-boundary value problems formulated on the basis of the usual theory. The multiplicity of solutions at the continuum level can be viewed as arising from a constitutive deficiency, reflecting the need to specify *additional* pieces of constitutive information.

One way to remedy this deficiency is to add two notions from materials science in the continuum setting: a nucleation criterion for the initiation of phase transition and a kinetic relation between interface velocity and the driving force of phase transformation (see for instance Truskinovsky, 1987; Abeyaratne and Knowles, 1991a). These relations can take into account the *internal dissipation* due to phase transitions. *A second way*, is to augment the elastic non-monotone theory by incorporating rate effects of Kelvin–Voigt type (James, 1980; Pego, 1987; Vainchtein and Rosakis, 1999), and/or effects due to the gradient of strain (Slemrod, 1983; Truskinovsky, 1985; Abeyaratne and Knowles, 1991b; Ngan and Truskinovsky, 2002). An augmented theory of this kind possesses its own kinetics due to the dissipative viscous mechanisms incorporated.

A different rate-type approach of the non-monotone elasticity based on a Maxwell's type viscosity has been considered for phase transition phenomena by Suliciu (1989b) and investigated, for instance, in Făciu

and Mihăilescu-Suliciu (1987), Suliciu (1990), Suliciu (1992), Făciu and Suliciu (1994), Făciu (1996) (see also the literature therein). In these papers it was shown that this isothermal model can describe phenomenologically many aspects encountered in the transformation pseudo-elasticity such as the hysteretic behavior in quasi-static strain- or stress-controlled experiments and the nucleation and growth of one phase into another. Recently, in order to model thermal effects which accompany phase transitions in shape memory alloys, Făciu and Mihăilescu-Suliciu (2002) have extended the isothermal Maxwelian rate-type model by taking into account the dependence on temperature of the non-monotone stress–strain relation. It was shown that this model successfully captures in quasi-static experiments the nucleation and evolution of deformation fronts and the corresponding distribution of temperature fields observed in the laboratory experiments performed by Shaw and Kyriakides (1997).

In order to do the proposed comparative investigation, in Part I of this paper we perform a *detailed* analysis of the wave structure for the elastic model equipped with a corresponding viscosity criterion for admissible solutions, since it is missing in the literature, while Part II is addressed to the wave structure analysis of the rate-type model. We investigate this problem in an one-dimensional and isothermal setting since this study can provide an important insight into the wave structure and can help to interpret laboratory results on phase transforming materials. In a future work, we extend the analysis to account for thermal effects.

The paper begins in Section 2 with a brief overview of the balance laws as well as the dissipation inequality for smooth and discontinuous fields. In Section 3, based on experimental facts for shape memory alloys (Otsuka et al., 1976) we describe the constitutive assumptions for a solid which can exist in three phases: a parent phase (austenite) and two variants of martensite. Some aspects related to the non-unicity of weak solutions for the elastic system are reminded. We propose a general rate-type constitutive equation which includes viscosity, a rate sensitivity parameter and an instantaneous response of the material as a convenient alternative for the description of dynamic phase transitions in a three phase material. Moreover, this formulation includes both the Maxwellian rate-type model when the dynamic Young modulus is finite and, as a limiting case when the dynamic Young modulus becomes infinite a generalized form of the Kelvin–Voigt model, used to describe phase transition phenomena in a phase transforming bar by Pego (1987), Vainchtein and Rosakis (1999) and Ngan and Truskinovsky (2002). According to the travelling waves analysis performed in Part II, by using our general rate-type approach, we obtain that a propagating strain discontinuity for the elastic system is admissible if and only if the well known chord criterion is satisfied, while any stationary strain discontinuity is unconditionally admissible.

In Section 4 we consider the simplest initial and boundary value problems for the elastic system, i.e., the Goursat problems. We determine, using the viscosity criterion, the wave propagation solutions to the complete set of Goursat problems which could arise as a result of dynamic interactions. The unique solutions of these problems are used as building blocks in solving the Riemann problems for all possible initial data. In Section 5 we use our Riemann solvers to construct exact solutions for the longitudinal impact of two elastic phase transforming bars. Thus, we consider at the initial moment a bar called "target" impacted at one end by another bar called "flyer" which is moving with a constant velocity V_0. After impact the two bars remain in contact and move together until a time t_S called time of separation. This time corresponds to the moment when the first tensile wave arrives at the point of contact. We determine critical values of the impact velocity such that a phase boundary be induced in the bars. We explore the interactions of the unloading elastic wave reflected at the rear end of the target with the phase boundary propagating inside the target and we determine critical values of the impact velocity such that this phase boundary propagates backward, or remains stationary or propagates forward after interaction. One focuses on two aspects which are precise indications for the appearance of a transformed zone at the contact point, the velocity time profile obtained at the free end of the target and the time of separation between the bars. For instance, we show that the transition from an elastic impact to a phase transforming impact induces an abrupt change of the time of separation between the two bars.

2. One-dimensional motion of thin bars

We consider a bar $\mathscr{B}$ with uniform cross-section and length L in an unstressed reference configuration which corresponds to a defined phase of the material. A longitudinal motion of the bar is characterized by a function $x = \chi(X,t)$ which gives the present position x of a particle in terms of the time t and its initial coordinate X in the reference configuration. The function $\chi(X,t)$ is assumed to be injective and bi-continuous with respect to X. Whenever $\chi(X,t)$ is differentiable we denote by $\varepsilon(X,t) = \frac{\partial \chi}{\partial X} - 1 > -1$ the strain at point X and by $v(X,t) = \frac{\partial \chi}{\partial t}$ the particle velocity.

In studying the propagation of longitudinal stress, strain and velocity waves in thin bars it is common to make a "one-dimensional" approximation in which the only non-vanishing stress component is the longitudinal one which is assumed to be uniform in a cross-section. Since the bar is thin, radial inertia effects are neglected. We denote by $\sigma = \sigma(X,t)$ the nominal stress (longitudinal force per unit area in the reference configuration). At points (X,t) where v, ε and σ are smooth functions the balance of momentum in the absence of body forces and the balance of mass have the form

$$\varrho \frac{\partial v}{\partial t} - \frac{\partial \sigma}{\partial X} = 0, \qquad \frac{\partial \varepsilon}{\partial t} - \frac{\partial v}{\partial X} = 0, \tag{1}$$

with ϱ being the (constant) mass density in the reference configuration.

If across a curve $X = S(t)$ in the (X,t)-plane at least one of the quantities v, ε, σ has jump discontinuities the balance of momentum and the continuity of the motion χ require

$$\varrho \dot{S}[v] + [\sigma] = 0, \qquad \dot{S}[\varepsilon] + [v] = 0, \tag{2}$$

where $\dot{S}(t)$ denotes the speed of propagation of the discontinuity, and for any function $f = f(X,t)$ we have used the notations $[f](t) = f^+(t) - f^-(t) = f(S(t)+,t) - f(S(t)-,t)$. Such a curve is usually called *a strain discontinuity* (or strong discontinuity). Let us note that independently of any constitutive assumption a *stationary strain discontinuity* is one for which

$$[\sigma] = 0, \quad [v] = 0, \quad [\varepsilon] \neq 0 \quad \text{and} \quad \dot{S} = 0, \tag{3}$$

while a *propagating strain discontinuity* is one for which

$$[\sigma] \neq 0, \quad [v] \neq 0, \quad [\varepsilon] \neq 0 \quad \text{and} \quad \varrho \dot{S}^2 = \frac{[\sigma]}{[\varepsilon]} > 0. \tag{4}$$

The second law of thermodynamics in this isothermal setting requires that the constitutive assumptions have to be compatible with the inequality

$$\varrho \dot{\psi} \leqslant \sigma \dot{\varepsilon}. \tag{5}$$

where ψ is the (Helmholtz) free energy function.

Inequality (5) is equivalent with

$$\varrho \frac{\partial}{\partial t}\left(\psi + \frac{1}{2}v^2\right) \leqslant \frac{\partial}{\partial X}(\sigma v), \tag{6}$$

wherefrom we get that across a strain discontinuity the following *dissipation inequality* has to be satisfied

$$D = \dot{S}(t)\left(\varrho[\psi] - \frac{\sigma^+ + \sigma^-}{2}[\varepsilon]\right) \geqslant 0. \tag{7}$$

Let us note that across a stationary strain discontinuity the dissipation inequality is always satisfied and moreover, there is no dissipation.

3. Constitutive assumptions—three phase materials

Starting with the paper by Ericksen (1975) the theory of elasticity with non-monotonic stress–strain relation $\sigma = \sigma_{\text{eq}}(\varepsilon)$, or equivalently with non-convex free energy function, has been used to describe the main features of phase transformations in solids (see for example, James, 1980, 1981; Abeyaratne and Knowles, 1991a,b, 1993; Pence, 1992, and the literature therein).

For a three-phase elastic material the simplest non-monotonic stress–strain relation is given by

$$\sigma = \sigma_{\text{eq}}(\varepsilon) = \begin{cases} E_3\varepsilon - \sigma_3 & \text{for } \varepsilon_m \leqslant \varepsilon \\ -E_2\varepsilon + \sigma_2 & \text{for } \varepsilon_a < \varepsilon < \varepsilon_m \\ E_1\varepsilon & \text{for } -\varepsilon_a \leqslant \varepsilon \leqslant \varepsilon_a \\ -E_2\varepsilon - \sigma_2 & \text{for } -\varepsilon_m < \varepsilon < -\varepsilon_a \\ E_3\varepsilon + \sigma_3 & \text{for } \varepsilon \leqslant -\varepsilon_m \end{cases} \tag{8}$$

where in Fig. 1

$$\sigma_a = E_1\varepsilon_a > 0, \quad \sigma_m = -E_2(\varepsilon_m - \varepsilon_a) + E_1\varepsilon_a, \quad 0 < \varepsilon_a < \varepsilon_m,$$
$$\sigma_2 = (E_1 + E_2)\varepsilon_a > 0, \quad \sigma_3 = (E_3 + E_2)\varepsilon_m - (E_1 + E_2)\varepsilon_a = E_3\varepsilon_m - \sigma_m.$$

This constitutive relation is viewed as corresponding to a material which can exist in an *austenite phase* and in two *variants of martensite*. $E_1 = \text{const.} > 0$ is called the elastic modulus of the austenite phase, while $E_3 = \text{const.} > 0$ is the elastic modulus of the martensite phase since the variants of martensite are crystallographically equivalent. $-E_2 = \text{const.} < 0$ is called the softening modulus and it corresponds to the unstable phases of the material.

Indeed, relation (8) reflects some experimental facts on materials capable of existing in more than one solid phase as shape memory alloys for instance (Otsuka et al., 1976). Thus, during a uniaxial test of an oriented single crystal specimen the material is found to remain in the austenite phase (cubic lattice) for sufficiently small values of the strain, in a martensitic variant (orthorhombic lattice with long side of crystal parallel to the tensile axis) for sufficiently large tensile strain and in an another orthorombic martensitic variant (orthorombic lattice with the long side of the crystal normal to the tensile axis) for sufficiently large compressive strain.

Thus, according to relation (8) we say that a particle X at a time t is in the *austenitic* phase $\mathscr{A}$, or in the *martensitic* variants $\mathscr{M}^+$, or $\mathscr{M}^-$ if the value of $\varepsilon(X,t)$ lies in the interval $[-\varepsilon_a, \varepsilon_a]$, or $[\varepsilon_m, \infty)$, or $(-1, -\varepsilon_m]$,

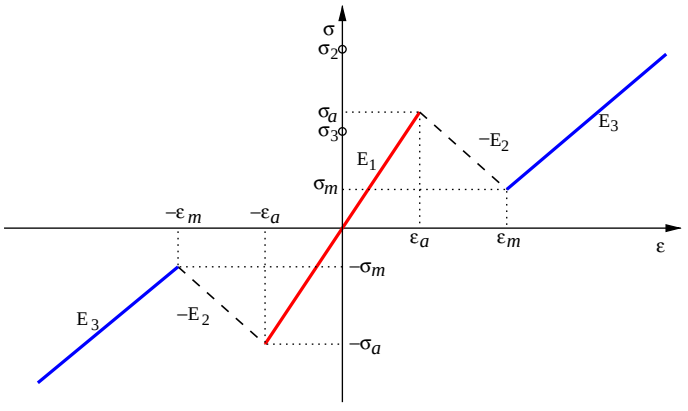

Fig. 1. The three phase elastic material: $\sigma = \sigma_{\text{eq}}(\varepsilon)$.

respectively. If $\varepsilon(X,t)$ belongs to $(\varepsilon_a,\varepsilon_m)$, or $(-\varepsilon_m,-\varepsilon_a)$, we say that the particle is in the unstable phases (spinodal regions) $\mathscr{I}^+$, or $\mathscr{I}^-$, respectively.

In the present setting *a strain discontinuity* may be now either an *elastic shock wave*, or a (propagating or stationary) *phase boundary*, according to whether the particles separated by the discontinuity are in the same phase, or in distinct phases.

Let us note that the second law of thermodynamics (5) ensures for *the elastic model* the existence of a unique (modulo a constant) free energy function $\psi=\psi_{\mathrm{eq}}(\varepsilon)$ with the property

$$\sigma_{\mathrm{eq}}(\varepsilon)=\varrho\frac{\mathrm{d}\psi_{\mathrm{eq}}(\varepsilon)}{\mathrm{d}\varepsilon},\quad \varepsilon>-1, \tag{9}$$

and leads to a null dissipation for any smooth field ε. On the other side, according to (7) for any strain jump the following *entropy inequality* has to be satisfied

$$D_{\mathrm{El}}(\varepsilon^+,\varepsilon^-)=\dot{S}A(\varepsilon^+,\varepsilon^-)=\dot{S}\left(\int_{\varepsilon^-}^{\varepsilon^+}\sigma_{\mathrm{eq}}(s)\mathrm{d}s-\frac{\sigma_{\mathrm{eq}}(\varepsilon^+)+\sigma_{\mathrm{eq}}(\varepsilon^-)}{2}(\varepsilon^+-\varepsilon^-)\right)\geqslant 0. \tag{10}$$

Therefore, a dissipation can be induced by a propagating strain discontinuity. In other words, strain discontinuities constitute sources of dissipation in elastic nonlinear materials. It is useful to observe that $A(\varepsilon^+,\varepsilon^-)$ is just the signed area between the graph of $\sigma_{\mathrm{eq}}(\varepsilon)$ and the chord which joins $(\varepsilon^-,\sigma_{\mathrm{eq}}(\varepsilon^-))$ with $(\varepsilon^+,\sigma_{\mathrm{eq}}(\varepsilon^+))$.

Let us also note that the elastodynamic system (1) and (8) is now of mixed type, i.e., hyperbolic for $\varepsilon\in(-1,-\varepsilon_m]\cup[-\varepsilon_a,\varepsilon_a]\cup[\varepsilon_m,\infty)$ and elliptic for $\varepsilon\in(-\varepsilon_m,-\varepsilon_a)\cup(\varepsilon_a,\varepsilon_m)$. Therefore, from mathematical point of view the Cauchy problem is ill-posed in the sense of Hadamard in the elliptic unstable regime, i.e., when phase transitions are involved. From physical point of view this is a strong indication of a constitutive deficiency of the dynamic non-monotone elasticity which suggests that additional constitutive information are needed.

Indeed, as in the case of monotone nonlinear elastic model there is a lack of uniqueness of the weak solutions for initial-boundary value problems. That is caused by the fact that jump conditions (2) admit too many solutions of which only some have physical meaning. Additional conditions termed *admissibility criteria*, are therefore sought to eliminate physically inadmissible solutions.

Similar to gas dynamics, for materials for which stress is strictly convex or strictly concave but monotonically increasing function of strain, the entropy inequality at shock fronts (10) is sufficient to ensure uniqueness of weak solutions to the Cauchy problem for the corresponding system of conservation law (see for instance Lax, 1971).

For a *non-monotone* elastic constitutive law the dissipation inequality (10) across a strong discontinuity is no longer sufficient to deliver uniqueness for the Cauchy problem, that is the entropy admissibility criterion is too weak. This situation reflects in fact the uncomplete physical description of phase transition phenomena by the non-monotone elasticity. Since the motion of a phase boundary is a strongly dissipative process, a dissipative mechanism has to be incorporated in the constitutive description. *One way* to remedy this deficiency, both in quasi-static and dynamic cases, is to supplement relation (8) with a kinetic relation that controls the rate at which the phase transition proceeds and of a nucleation criterion (see for instance Truskinovsky (1987), Abeyaratne and Knowles (1991a) and the literature therein). *A second alternative way*, which has a long tradition, to resolving this constitutive insufficiency is to embed the elastic bar theory as a special case of a broader theory which usually include viscosity of Kelvin–Voigt type and/or strain gradient effects (see for instance James (1980), Slemrod (1983), Pego (1987), Abeyaratne and Knowles (1991b), Ngan and Truskinovsky (2002) and the literature therein). An additional advantage of this second approach is that it does not require a separate nucleation criterion. Moreover, it possesses its own kinetics, since the material instability phenomena incorporated automatically lead to the formation and evolution of phase boundaries.

We adopt in this paper the second point of view mentioned above and we will consider instead of (8) an augmented theory described by the following general Maxwellian rate-type constitutive equation

$$\frac{\partial\sigma}{\partial t} - E\frac{\partial\varepsilon}{\partial t} = -\frac{E}{\mu}|\sigma - \sigma_{\mathrm{eq}}(\varepsilon)|^{\lambda-1}(\sigma - \sigma_{\mathrm{eq}}(\varepsilon)), \tag{11}$$

where $\sigma_{\mathrm{eq}}(\varepsilon)$ is a non-monotone stress–strain relation of type (8) called *the equilibrium curve* of the rate-type model. $E = \text{const.} > 0$ is the *dynamic Young modulus*, $\lambda = \text{const.} > 0$ is a *rate sensitivity parameter* and $\mu = \text{const.} > 0$ is a *viscosity coefficient*. For $\lambda = 1$, μ is a *Newtonian viscosity coefficient*, $\frac{\mu}{E}$ is a *relaxation time* of the model (of kinetic origin), while $k = \frac{E}{\mu}$ is usually called *Maxwellian viscosity coefficient*. When $\mu \to 0$ this rate-type constitutive equation can be seen as a rate-type approach of the elastic model in a sense which will be presented in the second part of this paper (Făciu and Molinari, 2005).

This rate-type constitutive equation has the capacity to describe the kinetics of phase transformation and it has been investigated in quasi-static experiments by Suliciu (1992), Făciu and Suliciu (1994) and Făciu (1996). As we illustrate in Part II, the new parameters μ, λ and E describe in fact the kinetics of the growth of phases and should be connected with the time of growth, or time of nucleation of microscopic theories of phase transitions. The constitutive relation (11) includes as a limiting case for $E \to \infty$ and $\lambda = 1$ the Kelvin–Voigt viscoelastic model which has been considered by James (1980), latter by Pego (1987) and recently by Vainchtein and Rosakis (1999) in relation with phase transformations in solids.

In investigating propagating phase boundaries in elastic fluids or solids some admissibility criteria intended to generalize the entropy inequality and designed to select physically relevant solutions have been proposed. For instance, Dafermos (1973) and Hattori (1986) proposed and used a maximum entropy rate admissibility condition. Slemrod (1983) derived admissibility conditions by embedding the theory of van der Waals fluid in a higher order theory that includes the effects of both viscosity and capillarity. James (1980) and Pego (1987), by using a Kelvin–Voigt viscosity approach, have studied the implications of such conditions in the setting of elastic bar theory. Suliciu (1989a, 1990) used a Maxwellian viscosity approach for a van der Waals fluid.

In this context, the problem of the stable, unstable or of the so-called "metastable states" and their nucleation, is still an open one. Indeed, while the entropy admissibility criterion is too weak in this case, the standard Kelvin–Voigt viscosity criterion (discussed by James, 1980; Slemrod, 1983; and Pego, 1987) is considered by some authors as too restrictive (strong) since it rules out propagating phase boundaries near the equilibrium co-existence line. Therefore, they introduce some variants of gradient elasticity or capillarity effect (see for instance Truskinovsky (1985), Abeyaratne and Knowles (1991b), Ngan and Truskinovsky (2002) and the literature therein).

Since different selection criteria may furnish different unique solutions to a Cauchy problem, only systematic experimental investigations as for example those performed by Escobar and Clifton (1995) could decide which is the physical relevant one. Therefore, the main goal of this work is to study the predictions of the two constitutive models, the elastic and the rate-type one, when we consider the longitudinal impact of two phase transforming bars and to suggest an experimental investigation program which could clarify some aspects connected with the dynamic nucleation of phases.

4. Riemann and Goursat problems—viscosity criterion

In the isothermal context for van der Waals fluids, the Riemann problem has been discussed for example by Slemrod (1983), Hattori (1986) and Suliciu (1989a, 1990) while for non-monotone elasticity by James (1980), Pego (1987), Abeyaratne and Knowles (1991a) and Pence (1992).

An augmented theory which takes into account the internal dissipation is often called dissipative regularization of the elastic model. It introduces an internal structure in a phase boundary and replaces the

sharp interfaces by transition layers of finite thickness. A standard approach to derive a selection criterion for admissible waves within the elastic theory is to identify as admissible those waves which arise in the frame of the augmented theory in the limit of vanishing viscosity. This approach, investigated in the second part of this paper (Făciu and Molinari, 2005) asserts that a strong discontinuity for the elastic model is admissible if and only if the strains ε^- and ε^+ on either side of the discontinuity can be smoothly connected by a travelling wave constructed within the augmented theory. Our analysis establishes that the generalized Maxwell's type viscoelastic approach (11) leads to the same admissibility condition as that obtained by Pego (1987) using the Kelvin–Voigt viscoelastic constitutive equation.

This *viscosity admissibility criterion* asserts: (i) a propagating strain discontinuity ($\dot{S} \neq 0$) is admissible if *the chord criterion* is satisfied and (ii) a stationary discontinuity ($\dot{S} = 0$) is admissible unconditionally. The *chord condition* is fulfilled if and only if the chord which joins the points $(\varepsilon^+, \sigma_{eq}(\varepsilon^+))$ to $(\varepsilon^-, \sigma_{eq}(\varepsilon^-))$ lies *below* (*above*) the graph of $\sigma_{eq}(\varepsilon)$ when $(\varepsilon^+ - \varepsilon^-)\dot{S} > 0$ (or $(\varepsilon^+ - \varepsilon^-)\dot{S} < 0$) for ε between ε^+ and ε^- (see for instance Fig. 2).

In the present paper we consider a piece-wise linear equilibrium curve given by (8) where we suppose additionally that

$$E_1 \geqslant E_3 > \frac{\sigma_m + \sigma_a}{\varepsilon_m + \varepsilon_a} \equiv F > 0. \tag{12}$$

This situation is called the *subsonic case* (Fig. 2) since the speed of any admissible phase boundary will be always lower than the speed of propagation of the elastic shock waves of either of the homogeneous phases, i.e., $\varrho\dot{S}^2 < E_1$ and $\varrho\dot{S}^2 < E_3$. Let us note that usually for shape memory alloys $E_1 \geqslant E_3$. The *supersonic* cases $E_1 > F > E_3$ (Fig. 3a) and $F < E_1 < E_3$ (Fig. 3b) will be discussed elsewhere.

We suppose additionally that $\sigma_m > 0$, ruling out for the present purposes the possibility that the bar can be in the martensitic phase at zero stress.

We use the viscosity criterion as selection criterion for weak solutions of the elastic system and we construct the corresponding unique solutions. First, we solve the simplest initial-boundary value problem for the elastic system (1) + (8), i.e. the Goursat problem. These are building blocks in solving the Riemann problem for all possible initial data. We give the complete description of the solution of the Riemann problem in order to illustrate in Section 5 how it can be used in investigating a laboratory experiment, that

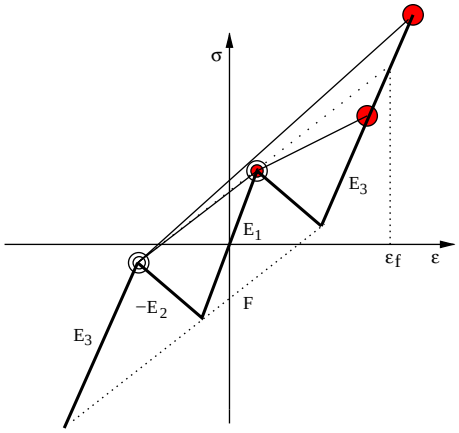

Fig. 2. Subsonic case $E_1 \geqslant E_3 > F$. Admissible waves connecting states $(\varepsilon^+, \sigma_{eq}(\varepsilon^+))$ (empty circle) and $(\varepsilon^-, \sigma_{eq}(\varepsilon^-))$ (filled circle) for $\varepsilon^+ < \varepsilon^-$ and $\dot{S} > 0$.

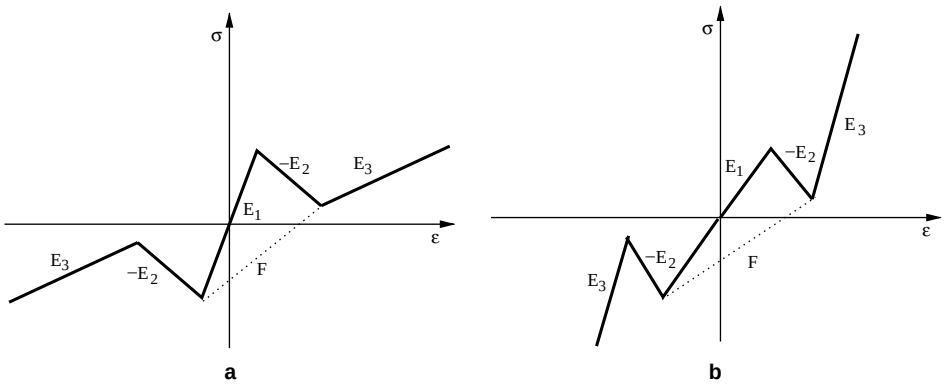

Fig. 3. (a) Supersonic case $E_1 > F > E_3$. (b) Supersonic case $F < E_1 < E_3$.

is the longitudinal impact of two phase transforming bars. Moreover, the solution of the Riemann problem is also a keystone in constructing a Godunov type numerical scheme for the elastic system (LeVeque, 1990).

4.1. The Goursat problems

The *right Goursat problem in stress* addresses wave propagation in a semi-infinite space $X > 0$ for the following initial and boundary condition

$$(\varepsilon, \sigma, v)(X, 0) = (\varepsilon_R, \sigma_R = \sigma_{\text{eq}}(\varepsilon_R), v_R), \text{ for } X > 0, \text{ and } \sigma(0, t) = \sigma^*, \text{ for } t > 0, \tag{13}$$

where ε_R, v_R and σ^* are given values.

Note that in the initial condition (13) it is superfluous to give the stress since this one is related to the strain through the elastic law (8). However, for the rate-type system (1) and (11), to be examined later, initial conditions have to include the stress. Thus the form (13) of initial condition is used for the homogeneity of the presentation.

As usual the solution is sought in the form of self-similar solutions, i.e., $(\varepsilon, \sigma, v)(X, t) = (\varepsilon, \sigma, v)(\xi)$, where $\xi = \frac{X}{t}$. The strong discontinuities have to satisfy jump conditions (2). We distinguish the following cases depending on the initial value ε_R and of the applied stress σ^*.

Case (M) $\varepsilon_R \in [\varepsilon_m, \infty)$—material initially in phase $\mathscr{M}^+$

$(\mathbf{M}_1)$ $\sigma^* \in [\sigma_m, \infty)$.

The material response is linear elastic with modulus E_3. The solution consists of an elastic shock wave $\frac{X}{t} = C_3 = \sqrt{\frac{E_3}{\varrho}}$ which separates the constant states $(\varepsilon_R, \sigma_R, v_R)$ and $(\varepsilon^*, \sigma^*, v^*)$ (see Fig. 4) where

$$v^* = v_R - \frac{\sigma^* - \sigma_R}{\varrho C_3}, \qquad \varepsilon^* = \frac{\sigma^* + \sigma_3}{E_3} > \varepsilon_m. \tag{14}$$

$(\mathbf{M}_2)$ $\sigma^* \in [-\sigma_a, \sigma_m)$.

According to the chord criterion there is a unique solution which consist of an elastic shock wave $\frac{X}{t} = C_3 = \sqrt{\frac{E_3}{\varrho}}$ which separates the constant states $(\varepsilon_R, \sigma_R, v_R)$ and $(\varepsilon_m, \sigma_m, v_m)$ and a phase boundary moving with the speed $C_p = \sqrt{\frac{E_1(\sigma^* - \sigma_m)}{\varrho(\sigma^* - E_1\varepsilon_m)}}$ which relates the states $(\varepsilon_m, \sigma_m, v_m)$ and $(\varepsilon^*, \sigma^*, v^*)$ (see Fig. 5) where

$$v_m = v_R - \frac{\sigma_m - \sigma_R}{\varrho C_3}, \; v^* = v_m + \frac{1}{\varrho C_3}\sqrt{(\sigma^* - \sigma_m)\left(\frac{E_3}{E_1}\sigma^* - \sigma_3 - \sigma_m\right)}, \; \varepsilon^* = \frac{\sigma^*}{E_1} < \frac{\sigma_m}{E_1}. \tag{15}$$

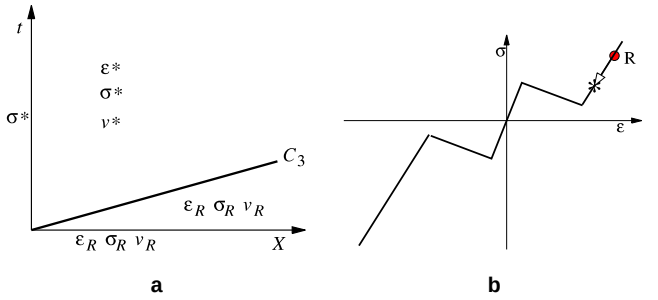

Fig. 4. Case $\mathbf{M}_1$: (a) Self-similar solution: elastic shock wave in phase $\mathscr{M}^+$. (b) Stress–strain states ahead and behind discontinuities.

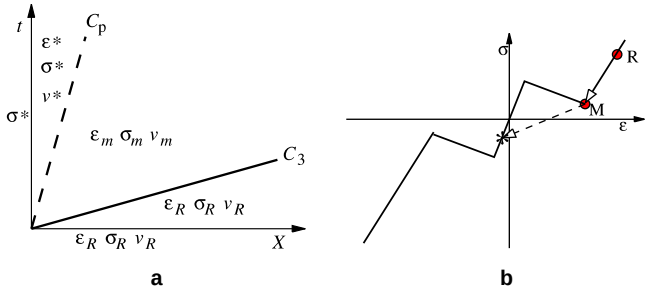

Fig. 5. Case $\mathbf{M}_2$: (a) Self-similar solution: Elastic shock wave precursor and a propagating phase boundary transforming the material from $\mathscr{M}^+$ to $\mathscr{A}$. (b) Stress–strain states ahead and behind discontinuities.

$(\mathbf{M}_3)$ $\sigma^* \in [-\sigma_f, -\sigma_a)$.

The pair $(-\varepsilon_f, -\sigma_f)$ corresponds to the intersection point between the graph of $\sigma = \sigma_{\text{eq}}(\varepsilon)$ and the straight line connecting the points $M(\varepsilon_m, \sigma_m)$ and $\overline{\text{A}}(-\varepsilon_a, -\sigma_a)$. According to the chord criterion we get the following wave structure. There is an elastic shock wave precursor $\frac{X}{t} = C_3$ which connects the constant states $(\varepsilon_R, \sigma_R, v_R)$ and $(\varepsilon_m, \sigma_m, v_m)$ and two propagating phase boundaries. The first one moves with the speed $C_f = \sqrt{\frac{\sigma_m+\sigma_a}{\varrho(\varepsilon_m+\varepsilon_a)}} = \sqrt{\frac{E}{\varrho}}$ and relates the states $(\varepsilon_m, \sigma_m, v_m)$ to $(-\varepsilon_a, -\sigma_a, \bar{v}_a)$ and corresponds to a $\mathscr{M}^+ \to \mathscr{A}$ phase transformation, while the second one moves with the speed $C_p = \sqrt{\frac{E_3(\sigma^*+\sigma_a)}{\varrho(\sigma^*-\sigma_3+E_3\varepsilon_a)}}$ and transforms the state $(-\varepsilon_a, -\sigma_a, \bar{v}_a)$ from phase $\mathscr{A}$ into $(\varepsilon^*, \sigma^*, v^*)$ in phase $\mathscr{M}^-$ (Fig. 6), where

$$\bar{v}_a = v_m + \frac{1}{\varrho C_f}(\sigma_a + \sigma_m), \quad v^* = \bar{v}_a + \frac{1}{\varrho C_3}\sqrt{(\sigma^* + \sigma_a)\left(\sigma^* - \sigma_3 + \frac{E_3}{E_1}\sigma_a\right)}, \quad \varepsilon^* = \frac{\sigma^* - \sigma_3}{E_3} > -\varepsilon_f. \tag{16}$$

$(\mathbf{M}_4)$ $\sigma^* \in (-\infty, -\sigma_f)$

The solution consists of an elastic shock wave precursor in $\mathscr{M}^+$ phase which separates the constant states $(\varepsilon_R, \sigma_R, v_R)$ and $(\varepsilon_m, \sigma_m, v_m)$ and of a phase boundary propagating with the speed $C_p = \sqrt{\frac{E_3(\sigma_m-\sigma^*)}{\varrho(2\sigma_3+\sigma_m-\sigma^*)}} > C_f$ which connects the constant states $(\varepsilon_m, \sigma_m, v_m)$ to $(\varepsilon^*, \sigma^*, v^*)$. It corresponds to an impact $\mathscr{M}^+ \to \mathscr{M}^-$ induced phase transformation (Fig. 7). Here

$$v^* = v_m + \frac{1}{\varrho C_3}\sqrt{(2\sigma_3 + \sigma_m - \sigma^*)(\sigma_m - \sigma^*)}, \quad \varepsilon^* = \frac{\sigma^* - \sigma_3}{E_3} < -\varepsilon_f. \tag{17}$$

Therefore, we can build two functions denoted H_R^M and G_R^M, which for given $(\varepsilon_R, \sigma_R, v_R), \varepsilon_R \geqslant \varepsilon_m$ associate to the applied stress $\sigma^* \in \mathbb{R}$ the velocity $v^* = v(0,t)$ and strain $\varepsilon^* = \varepsilon(0,t)$, solution of the Goursat problem (13) at the boundary $(X = 0, t > 0)$. By removing the index * these functions can be written as follows:

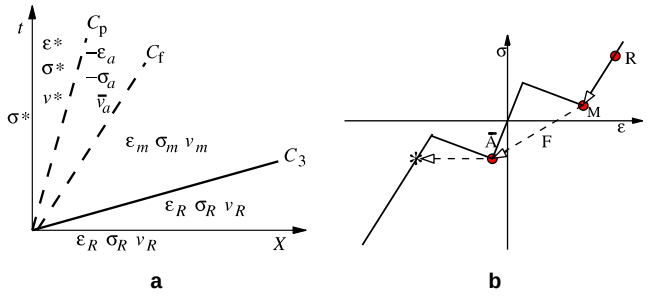

Fig. 6. Case $\mathbf{M}_3$: (a) Self-similar solution: Elastic shock wave precursor and two propagating phase boundaries transforming the material from $\mathscr{M}^+$ to $\mathscr{A}$ and from $\mathscr{A}$ to $\mathscr{M}^-$. (b) Stress–strain states ahead and behind discontinuities.

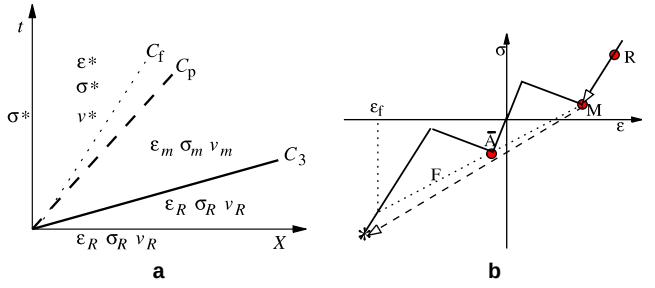

Fig. 7. Case $\mathbf{M}_4$: (a) Self-similar solution: elastic shock wave precursor and a high speed $\mathscr{M}^+ \to \mathscr{M}^-$ propagating phase boundary. (b) Stress–strain states ahead and behind discontinuities.

$$
\begin{aligned}
v =& H_R^M(\sigma;\varepsilon_R,\sigma_R = E_3\varepsilon_R - \sigma_3, v_R)\\
=& \begin{cases}
v_R - \frac{1}{\varrho C_3}(\sigma_m - \sigma_R) + \frac{1}{\varrho C_3}\sqrt{(\sigma-\sigma_m)(\sigma-\sigma_m-2\sigma_3)}, & \sigma < -\sigma_f,\\
v_R - \frac{1}{\varrho C_3}(\sigma_m - \sigma_R) + \frac{1}{\varrho C_f}(\sigma_m + \sigma_a) + \frac{1}{\varrho C_3}\sqrt{(\sigma+\sigma_a)\left(\sigma + \frac{E_3}{E_1}\sigma_a - \sigma_3\right)}, & -\sigma_f \leqslant \sigma < -\sigma_a,\\
v_R - \frac{1}{\varrho C_3}(\sigma_m - \sigma_R) + \frac{1}{\varrho C_3}\sqrt{(\sigma-\sigma_m)\left(\frac{E_3}{E_1}\sigma - \sigma_m - \sigma_3\right)}, & -\sigma_a \leqslant \sigma < \sigma_m,\\
v_R - \frac{1}{\varrho C_3}(\sigma - \sigma_R), & \sigma_m \leqslant \sigma
\end{cases}, \qquad (18)\\
\varepsilon =& G_R^M(\sigma;\varepsilon_R,\sigma_R = E_3\varepsilon_R - \sigma_3, v_R) = \begin{cases}
\frac{1}{E_3}(\sigma - \sigma_3), & \sigma < -\sigma_a\\
\frac{1}{E_1}\sigma, & -\sigma_a \leqslant \sigma < \sigma_m\\
\frac{1}{E_3}(\sigma + \sigma_3) & \sigma_m \leqslant \sigma
\end{cases}. \qquad (19)
\end{aligned}
$$

Note that function H_R^M is *a continuous and strictly decreasing* function of σ, thus it is invertible. At points $\sigma = \sigma_m$ and $\sigma = -\sigma_a$ the graph presents angular points with left and right vertical slopes. On the other side, function G_R^M is discontinuous at σ_m and $-\sigma_a$. This property reflects the strain intervals which are not allowed for a phase transformation by the chord criterion.

We can also consider *the right Goursat problem in velocity* when instead of giving σ^* at $X = 0$ for $t > 0$ in (13) we prescribe a constant velocity v^*. It is obvious that this problem has a unique solution too, which follows immediately by using functions H_R^M and G_R^M due to the one-to-one correspondence between v^*

and σ^*. Let us note that the wave structure can be also immediately determined using the properties of functions H_R^M and G_R^M.

Case (A) $\varepsilon_R \in [-\varepsilon_a, \varepsilon_a]$—material initially in phase $\mathscr{A}$

The wave structure is again determined by using jump relations (2) and the chord criterion. We write here only the functions H_R^A and G_R^A which for fixed initial data $\varepsilon_R, \sigma_R = E_1\varepsilon_R, v_R$ associate to an applied stress σ^* the values v^* and ε^*, where $v^* = v(0,t)$ and $\varepsilon^* = \varepsilon(0,t)$ for $t > 0$. By removing again the superscript * we have:

$$v = H_R^A(\sigma; \varepsilon_R, \sigma_R = E_1\varepsilon_R, v_R) = \begin{cases} v_R + \frac{1}{\varrho C_1}(\sigma_R + \sigma_a) + \frac{1}{\varrho C_3}\sqrt{(\sigma + \sigma_a)\left(\sigma - \sigma_3 + \frac{E_3}{E_1}\sigma_a\right)}, & \sigma < -\sigma_a, \\ v_R - \frac{1}{\varrho C_1}(\sigma - \sigma_R), & -\sigma_a \leqslant \sigma < \sigma_a, \\ v_R + \frac{1}{\varrho C_1}(\sigma_R - \sigma_a) - \frac{1}{\varrho C_3}\sqrt{(\sigma - \sigma_a)\left(\sigma + \sigma_3 - \frac{E_3}{E_1}\sigma_a\right)}, & \sigma_a < \sigma, \end{cases} \tag{20}$$

$$\varepsilon = G_R^A(\sigma; \varepsilon_R, \sigma_R = E_1\varepsilon_R, v_R) = \begin{cases} \frac{1}{E_3}(\sigma - \sigma_3), & \sigma < -\sigma_a, \\ \frac{1}{E_1}\sigma, & -\sigma_a \leqslant \sigma \leqslant \sigma_a, \\ \frac{1}{E_3}(\sigma + \sigma_3), & \sigma_a < \sigma. \end{cases} \tag{21}$$

Reciprocally, by knowing functions H_R^A and G_R^A and the position of σ with respect to $-\sigma_a$ and σ_a we can immediately determine the wave structure of the Goursat problem. Thus, if $\sigma > \sigma_a$ the impact produces an elastic shock wave in austenitic phase propagating with speed $C_1 = \sqrt{E_1/\varrho}$ and a phase boundary propagating with speed $C_p(\sigma) = \sqrt{\frac{(\sigma-\sigma_a)}{\varrho(G_R^A(\sigma)-\varepsilon_a)}}$ transforming the material from phase $\mathscr{A}$ to phase $\mathscr{M}^+$ (Fig. 8a and b). If $\sigma \in [-\sigma_a, \sigma_a]$ then the impact condition leads to an elastic shock wave in austenitic phase propagating with speed $C_1 = \sqrt{E_1/\varrho}$ (Fig. 8c and d). If $\sigma < -\sigma_a$ we get an elastic shock wave precursor with speed $C_1 = \sqrt{E_1/\varrho}$ and a phase boundary propagating with speed $C_p(\sigma) = \sqrt{\frac{(\sigma+\sigma_a)}{\varrho(G_R^A(\sigma)+\varepsilon_a)}}$ transforming the material from phase $\mathscr{A}$ to phase $\mathscr{M}^-$ (Fig. 8e and f).

Let us note that H_R^A is also a *continuous and strictly decreasing* function of σ realizing a one-to-one correspondence between the applied stress σ^* and the resulting velocity v^* at the boundary ($X = 0, t > 0$). As a consequence the *right Goursat problem in velocity* has a unique solution, too. On the other side, function G_R^A has a finite jump at points σ_a and $-\sigma_a$, describing in this way the strain intervals which are not allowed by the transformation according to the chord criterion.

Case ($\overline{\mathbf{M}}$) $\varepsilon_R \in (-1, -\varepsilon_m]$—material initially in phase $\mathscr{M}^-$

The solution is obtained in a similar way as in the case (**M**). We write here only the functions $H_R^{\overline{M}}$ and $G_R^{\overline{M}}$ which for fixed initial data $(\varepsilon_R, \sigma_{eq}(\varepsilon_R) = E_3\varepsilon_R + \sigma_3, v_R)$ associate to an applied stress σ^* the values v^* and ε^* where $v^* = v(0,t)$ and $\varepsilon^* = \varepsilon(0,t)$ for $t > 0$. These are:

$$\begin{aligned} v =& H_R^{\overline{M}}(\sigma; \varepsilon_R, \sigma_R = E_3\varepsilon_R + \sigma_3, v_R) \\ =& \begin{cases} v_R - \frac{1}{\varrho C_3}(\sigma - \sigma_R), & \sigma \leqslant -\sigma_m \\ v_R + \frac{1}{\varrho C_3}(\sigma_m + \sigma_R) - \frac{1}{\varrho C_3}\sqrt{(\sigma + \sigma_m)\left(\frac{E_3}{E_1}\sigma + \sigma_m + \sigma_3\right)}, & -\sigma_m < \sigma \leqslant \sigma_a \\ v_R + \frac{1}{\varrho C_3}(\sigma_m + \sigma_R) - \frac{1}{\varrho C_f}(\sigma_m + \sigma_a) - \frac{1}{\varrho C_3}\sqrt{(\sigma - \sigma_a)\left(\sigma - \frac{E_3}{E_1}\sigma_a + \sigma_3\right)}, & \sigma_a < \sigma \leqslant \sigma_f \\ v_R + \frac{1}{\varrho C_3}(\sigma_m + \sigma_R) - \frac{1}{\varrho C_3}\sqrt{(\sigma + \sigma_m)(\sigma + \sigma_m + 2\sigma_3)}, & \sigma_f < \sigma \end{cases} \end{aligned} \tag{22}$$

$$\varepsilon = G_R^{\overline{M}}(\sigma; \varepsilon_R, \sigma_R = E_3\varepsilon_R + \sigma_3, v_R) = \begin{cases} \frac{1}{E_3}(\sigma - \sigma_3), & \sigma \leqslant -\sigma_m \\ \frac{1}{E_1}\sigma, & -\sigma_m < \sigma \leqslant \sigma_a \\ \frac{1}{E_3}(\sigma + \sigma_3), & \sigma_a < \sigma \end{cases} \tag{23}$$

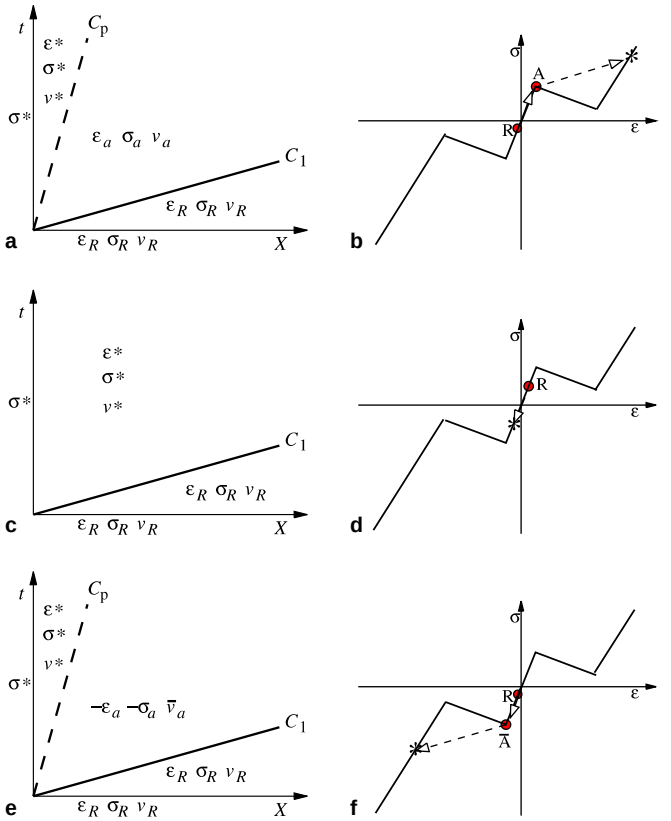

Fig. 8. Case **A**: (a), (c), (e) Self-similar solutions. (b), (d), (f) Stress–strain states ahead and behind discontinuities.

From relations (22) and (23) we can read the following wave structure. If $\sigma \leqslant -\sigma_m$ there is only an elastic shock wave propagating with the speed C_3. If $\sigma \in (-\sigma_m, \sigma_a]$ there is an elastic shock wave precursor which propagates with speed C_3 into the semi-infinite space $X > 0$ followed by a $\mathscr{M}^- \to A$ transformation front propagating with the speed $C_p(\sigma) = \sqrt{\frac{E_1(\sigma+\sigma_m)}{\varrho(\sigma+E_1\varepsilon_m)}}$. When $\sigma \in (\sigma_a, \sigma_f]$, then an elastic shock wave in the $\mathscr{M}^-$ phase is followed by two transformation fronts. The first one propagates with the speed $C_f = \sqrt{\frac{(\sigma_m+\sigma_a)}{\varrho(\varepsilon_m+\varepsilon_a)}}$ transforming the material from phase $\mathscr{M}^-$ to phase $\mathscr{A}$. The second one propagates with the speed $C_p(\sigma) = \sqrt{\frac{E_3(\sigma-\sigma_a)}{\varrho(\sigma+\sigma_3-E_3\varepsilon_a)}} < C_f$ and transforms the material from the austenite state (ε_a,σ_a) to a state in $\mathscr{M}^-$ phase. When $\sigma > \sigma_f$ then the elastic shock wave precursor in the $\mathscr{M}^-$ phase is followed by a high speed propagating phase boundary $C_p(\sigma) = \sqrt{\frac{E_3(\sigma+\sigma_m)}{\varrho(\sigma+\sigma_3+E_3\varepsilon_m)}} > C_f$ which transforms directly the material from $\mathscr{M}^-$ to $\mathscr{M}^+$ phase.

Let us note that function $H_R^{\overline{M}}$ is a *continuous and strictly decreasing* function of σ, thus being invertible. At the points $\sigma = -\sigma_m$ and $\sigma = \sigma_a$ the graph presents angular points with right vertical slopes. On the other side, function G_R^M is discontinuous at σ_m and $-\sigma_a$ thus reflecting the nature of the phase transformation according to the chord criterion.

The solution of the *left Goursat problem in stress*

$$(\varepsilon, \sigma, v)(X, 0) = (\varepsilon_L, \sigma_L = \sigma_{\text{eq}}(\varepsilon_L), v_L), \text{ for } X < 0, \text{ and } \sigma(0, t) = \sigma^*, \text{ for } t > 0, \tag{24}$$

where ε_L,v_L and σ^* are given values, can be constructed in the same way as for the right one. The expression of the functions $v^* = H_L^i(\sigma^*; \varepsilon_L, \sigma_L = \sigma_{eq}(\varepsilon_L), v_L)$ and $\varepsilon^* = G_L^i(\sigma; \varepsilon_L, \sigma_L = \sigma_{eq}(\varepsilon_L), v_L), i \in \{\overline{M}, A, M\}$ which associate to the constant boundary condition σ^* the values $v^* = v(0,t)$ and $\varepsilon^* = \varepsilon(0,t)$ for $t > 0$, respectively, are obtained from relations (18)–(23) by replacing R into L, C_1 into $-C_1$, C_3 into $-C_3$, C_f into $-C_f$ and C_p into $-C_p$. In this case the curves $v^* = H_L^i(\sigma^*; \varepsilon_L, \sigma_L = \sigma_{eq}(\varepsilon_L), v_L), i \in \{\overline{M}, A, M\}$ are *continuous and strictly increasing*, being thus *invertible*. As a consequence the *left Goursat problem in velocity* has always a unique solution, too.

4.2. The Riemann problem

The Riemann problem consists in finding the weak solutions of the elastic system (1) and (8) in the half plane $t > 0$ of the (X,t)-plane that satisfies the following conditions

$$\begin{aligned} (\varepsilon, \sigma, v)(X,0) &= (\varepsilon_L, \sigma_L = \sigma_{eq}(\varepsilon_L), v_L) \quad \text{for } X < 0, \\ (\varepsilon, \sigma, v)(X,0) &= (\varepsilon_R, \sigma_R = \sigma_{eq}(\varepsilon_R), v_R) \quad \text{for } X > 0, \end{aligned} \tag{25}$$

where (ε_L,v_L) and (ε_R,v_R) are given values.

We can view the Riemann problem as consisting of two Goursat problems, a right and a left one, submitted to the condition that across the material surface $X = 0$ the stress and the velocity coincide for $t > 0$. Indeed, according to relations (3) only the strain may suffer a jump discontinuity across the vertical line $X = 0$, allowing us to describe stationary phase boundaries.

The solution of the Riemann problem is obtained by intersecting in the σ–v plane the curves $v = H_L^i(\sigma; \varepsilon_L, \sigma_L = \sigma_{eq}(\varepsilon_L), v_L)$ and $v = H_R^i(\sigma; \varepsilon_R, \sigma_R = \sigma_{eq}(\varepsilon_R), v_R)$, $i \in \{\overline{M}, A, M\}$ which pass through the points (σ_R,v_R) and (σ_L,v_L), respectively. Since the first one is strictly decreasing and the second one is strictly increasing it follows that they meet always each other in a single point (σ^*, v^*). Thus the uniqueness of the solution of the Goursat problems ensures the uniqueness of the solution of the Riemann problems with respect to the chord criterion. Moreover, as we have already seen in the previous section, the form of the graphs of functions $v = H_L^i(\sigma; \varepsilon_L, \sigma_L = \sigma_{eq}(\varepsilon_L), v_L)$ and $v = H_R^i(\sigma; \varepsilon_R, \sigma_R = \sigma_{eq}(\varepsilon_R), v_R)$ contains the wave structure corresponding to the Riemann problem which can be read out easily. The procedure will be exemplified in the following when investigating the longitudinal impact of two bars.

5. Longitudinal impact of two bars—exact solution

Experiments with longitudinal impact of elastic and plastic bars have been intensively investigated in the sixtieth and seventieth years (see for instance Bell (1968), §4.28; Cristescu and Suliciu (1982), Chap. IV and the literature therein). Such kind of experiments can be used to study the kinetics of phase transformation in shape memory alloys, too (see for instance the pressure-shear plate experiments reported by Escobar and Clifton, 1995).

Consider two bars of the same phase transforming material. One called flyer (projectile bar) is shot out from an air gun with known velocity V_0, and travels freely to the right until it impinges a bar at rest called target. We denote by L the length of the flyer and by l the length of the target and we suppose $L > l$. The left end of the flyer and the right end of the target bar are stress free. After impact the two bars remain in contact and move together until a time t_S called *time of separation*. This time corresponds to the moment when the first tensile wave arrives at the point of contact $X = 0$. Indeed, since the two bars are not glued at the impact face $X = 0$ they can not support a dilatational wave and consequently they have to separate. After separation we have to consider at $X = 0$ free stress end conditions for both bars.

Thus, the initial-boundary value problem to be solved is the following:

$$(\varepsilon,\sigma,v)(X,0)=(0,0,V_0)\quad \text{for } X\in[-L,0],\ (\varepsilon,\sigma,v)(X,0)=(0,0,0)\quad \text{for } X\in(0,l], \tag{26}$$

$$\begin{aligned}&\sigma(-L,t)=0\quad \text{and } \sigma(l,t)=0,\quad \text{for}\quad t\geqslant 0,\\ &\sigma(0-,t)=\sigma(0+,t)\quad \text{and } v(0-,t)=v(0+,t),\quad \text{for}\quad t\in[0,t_S),\\ &\sigma(0-,t)=0\quad \text{and } \sigma(0+,t)=0,\quad \text{for}\quad t\geqslant t_S.\end{aligned} \tag{27}$$

The time t_S has to be determined when constructing the solution, being the first time when $\sigma(-,t)$ or $\sigma(0+,t)$ first becomes positive.

For simplicity we consider in the following the case $E_1=E_3$, i.e. the elastic modulus of the austenite phase $\mathscr{A}$ is equal with the elastic modulus of the martensite variants $\mathscr{M}^{\pm}$. In order to describe the solution of the initial-boundary value problem (26) and (27) for the elastic system (1) and (8) we use a time-distance diagram of wave propagation in the flyer and target after impact as in Fig. 10a or Fig. 11a. It is obvious that at time $t=0$ we have to solve a Riemann problem with the constant data (26) around $X=0$. The solution at $X=0$, $t>0$ and the wave structure is obtained by intersecting the fixed curve $v=H_R^A(\sigma;0,0,0)$ passing through the point ($\sigma=0$,$v=0$), given by (20), with the curve $v=H_L^A(\sigma;0,0,V_0)$, passing through the point ($\sigma=0$,$v=V_0$), obtained from the same formula by replacing C_1 to $-C_1$ and R to L, (Fig. 9), i.e.,

$$v=H_L^A(\sigma;0,0,V_0)=\begin{cases}V_0-\frac{1}{\sqrt{\varrho E_1}}\sigma_a-\frac{1}{\sqrt{\varrho E_1}}\sqrt{(\sigma+\sigma_a)(\sigma-\sigma_3+\sigma_a)}, & \sigma<-\sigma_a\\ V_0+\frac{1}{\sqrt{\varrho E_1}}\sigma, & -\sigma_a\leqslant\sigma\leqslant\sigma_a\\ V_0+\frac{1}{\sqrt{\varrho E_1}}\sigma_a+\frac{1}{\sqrt{\varrho E_1}}\sqrt{(\sigma-\sigma_a)(\sigma+\sigma_3-\sigma_a)}, & \sigma_a<\sigma\end{cases} \tag{28}$$

$$v=H_R^A(\sigma;0,0,0)=\begin{cases}\frac{1}{\sqrt{\varrho E_1}}\sigma_a+\frac{1}{\sqrt{\varrho E_1}}\sqrt{(\sigma+\sigma_a)(\sigma-\sigma_3+\sigma_a)}, & \sigma<-\sigma_a\\ -\frac{1}{\sqrt{\varrho E_1}}\sigma, & -\sigma_a\leqslant\sigma\leqslant\sigma_a\\ -\frac{1}{\sqrt{\varrho E_1}}\sigma_a-\frac{1}{\sqrt{\varrho E_1}}\sqrt{(\sigma-\sigma_a)(\sigma+\sigma_3-\sigma_a)}, & \sigma_a<\sigma\end{cases} \tag{29}$$

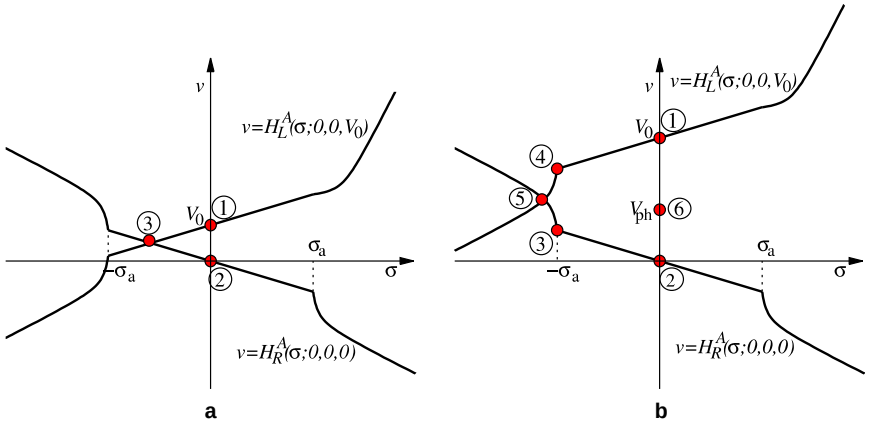

Fig. 9. Solution of the Riemann problem at $X=0$ and $t>0$. (a) Case $V_0\leqslant V_{\text{ph}}$—no phase transformation (encircled numbers correspond to Fig. 10a). (b) Case $V_0>V_{\text{ph}}$—impact-induced phase transformation (encircled numbers correspond to Fig. 11a).

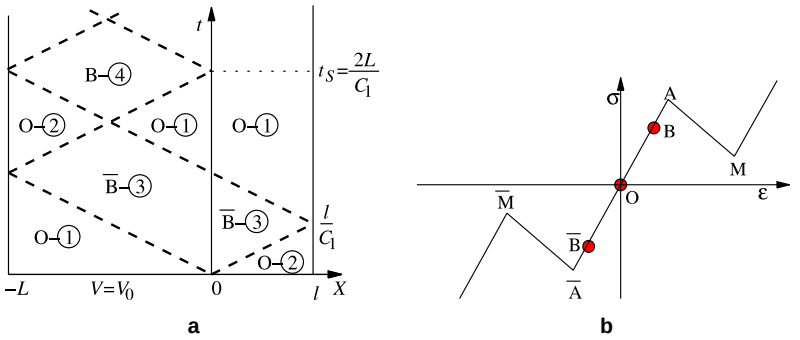

Fig. 10. Elastic linear impact ($V_0 \leqslant V_{\text{ph}}$). Capital letters denote stress–strain states; encircled numbers denote stress–velocity states in Fig. 9a. (a) t–X diagram, (b) stress–strain states ahead and behind discontinuities.

The impact-induced wave structure depends on the magnitude of the velocity V_0 of the projectile. It is important to note here that this appears linearly in the expression of function $v = H_L^A(\sigma; 0, 0, V_0)$.

(a) *Elastic impact*. If

$$V_0 \leqslant V_{\text{ph}} \equiv \frac{2\sigma_a}{\sqrt{\varrho E_1}} \tag{30}$$

the impact between the two bars is only elastic linear. Indeed, from (28) and (29) we get that condition (30) is equivalent with $H_L^A(-\sigma_a; 0, 0, V_0) < H_R^A(-\sigma_a; 0, 0, 0)$. Therefore, the two curves meet each other in their linear part (Fig. 9a) which means that the two bars behaves linearly elastic during the impact. The solution of problem (26) and (27) represented in the time-distance diagram Fig. 10a is:

$$\text{O-}① \leftrightarrow (\varepsilon = 0, \sigma = 0, v = V_0), \quad \text{O-}② \leftrightarrow (\varepsilon = 0, \sigma = 0, v = 0),$$
$$\overline{\text{B}}\text{-}③ \leftrightarrow \left(\varepsilon = -\frac{V_0}{2C_1}, \sigma = -\frac{\varrho C_1 V_0}{2}, V = \frac{V_0}{2}\right), \quad \text{B-}④ \leftrightarrow \left(\varepsilon = \frac{V_0}{2C_1}, \sigma = \frac{\varrho C_1 V_0}{2}, V = \frac{V_0}{2}\right).$$

The time of separation is $t_S = \frac{2L}{C_1}$ and corresponds to the arrival time of the elastic unloading wave reflected at $X = -L$.

(b) *Impact-induced phase transformation.* If

$$V_0 > V_{\text{ph}} \equiv \frac{2\sigma_a}{\sqrt{\varrho E_1}} \tag{31}$$

a phase transformation is induced in the neighborhood of the impact face. This result is in agreement with what experimentally is known, that is, if the impact velocity is sufficiently large a new phase nucleates and grows in the phase transforming material. In the case of the elastic model with chord condition as selection criterion this value is given by the critical value (31). It is thus obvious that, according to the viscosity criterion, the dynamic nucleation of a new phase is associated with the attainment of the maxima/minima of the equilibrium curve.

Indeed, condition (31) is equivalent with relation $H_L^A(-\sigma_a; 0, 0, V_0) > H_R^A(-\sigma_a; 0, 0, 0)$. One reads out easily from Fig. 9b that two elastic shock wave precursors propagating left and right with speed C_1 are followed by two symmetric propagating phase boundaries. The solution of the Riemann problem at the point O($t = 0, X = 0$) is described below and illustrated in Fig. 11. There are five regions in the X–t diagram where the solution is the following:

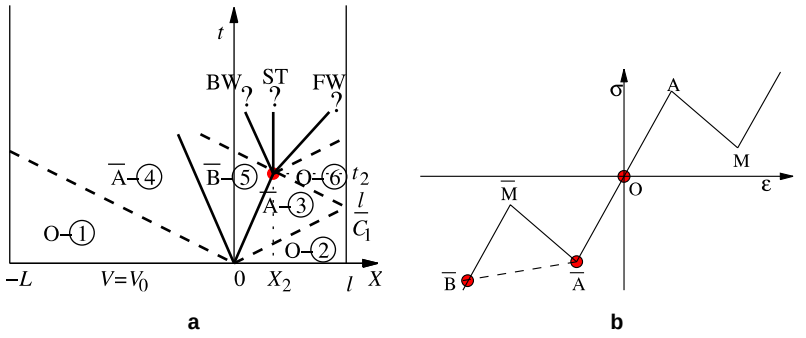

Fig. 11. Shock-induced phase transformation ($v > V_{\mathrm{ph}}$). Capital letters denote stress–strain states; encircled numbers denote stress–velocity states in Fig. 9b. (a) t–X diagram, (b) stresss–strain states ahead and behind discontinuities.

$$\overline{\mathrm{A}}\text{-}③ \leftrightarrow \left(\varepsilon = -\varepsilon_a, \sigma = -\sigma_a, v = \frac{V_{\mathrm{ph}}}{2}\right), \quad \overline{\mathrm{A}}\text{-}④ \leftrightarrow \left(\varepsilon = -\varepsilon_a, \sigma = -\sigma_a, v = V_0 - \frac{V_{\mathrm{ph}}}{2}\right),$$

$$\overline{\mathrm{B}}\text{-}⑤ \leftrightarrow \begin{cases} \varepsilon_{\overline{\mathrm{B}}}(\eta) = \frac{1}{E_1}(\sigma_{\overline{\mathrm{B}}}(\eta) - \sigma_3), & \varepsilon = -\frac{1}{E_1}(\sigma_a + \sigma_3) \\ \sigma_{\overline{\mathrm{B}}}(\eta) = -\sigma_a + \frac{1}{2}\sigma_3 - \frac{1}{2}\sqrt{\sigma_3^2 + \eta^2}, \quad \overset{\eta\to 0}{\to} & \sigma = -\sigma_a, \\ v = \frac{1}{2}V_{\mathrm{ph}} + \frac{1}{2\sqrt{\varrho E_1}}\eta = \frac{1}{2}V_0, & v = \frac{V_{\mathrm{ph}}}{2} \end{cases} \tag{32}$$

where

$$\eta \equiv \sqrt{\varrho E_1} V_0 - 2\sigma_a > 0.$$

The limiting case $\eta \to 0$ is analyzed in an explicit manner in (32) and in what follows.

The phase boundaries propagates left and right with the speed $P_1 < C_1$ given by relation

$$P_1^2(\eta) = \frac{E_1}{\varrho}\frac{\sqrt{\sigma_3^2 + \eta^2} - \sigma_3}{\sqrt{\sigma_3^2 + \eta^2} + \sigma_3} \overset{\eta\to 0}{\to} 0. \tag{33}$$

At time $t_1 = \frac{l}{C_1}$ an elastic compressive shock arrives at the rear surface of the target and reflects as an unloading wave (Fig. 11a). The solution in the adjacent region O-⑥ is determined as solution of a left Goursat problem with initial data $\overline{\mathrm{A}}$-③ and free stress end condition. We get

$$\mathrm{O}\text{-}⑥ \leftrightarrow (\varepsilon = 0, \sigma = 0, v = V_{\mathrm{ph}}). \tag{34}$$

The unloading shock wave intersects the right propagating phase boundary at the point $R_2(X_2, t_2)$, where

$$X_2(\eta) = \frac{2lP_1(\eta)}{C_1 + P_1(\eta)} \text{ and } t_2(\eta) = \frac{2l}{C_1 + P_1(\eta)} > t_1. \tag{35}$$

The question is what is the effect of this interaction. The answer is obtained by solving a Riemann problem with the left state $\overline{\mathrm{B}}$-⑤ and the right state $\overline{\mathrm{O}}$-⑥ (Fig. 11). The solution is obtained by intersecting the monotone increasing curve $v = H_L^{\overline{\mathrm{M}}}(\sigma; \varepsilon_{\overline{\mathrm{B}}}, \sigma_{\overline{\mathrm{B}}}, \frac{V_0}{2})$ passing through the point $(\sigma_{\overline{\mathrm{B}}}, \frac{V_0}{2})$ with the monotone decreasing curve $v = H_R^A(\sigma; 0, 0, V_{\mathrm{ph}})$ passing through the point $(0, V_{\mathrm{ph}})$, given by relations (20) and (22),

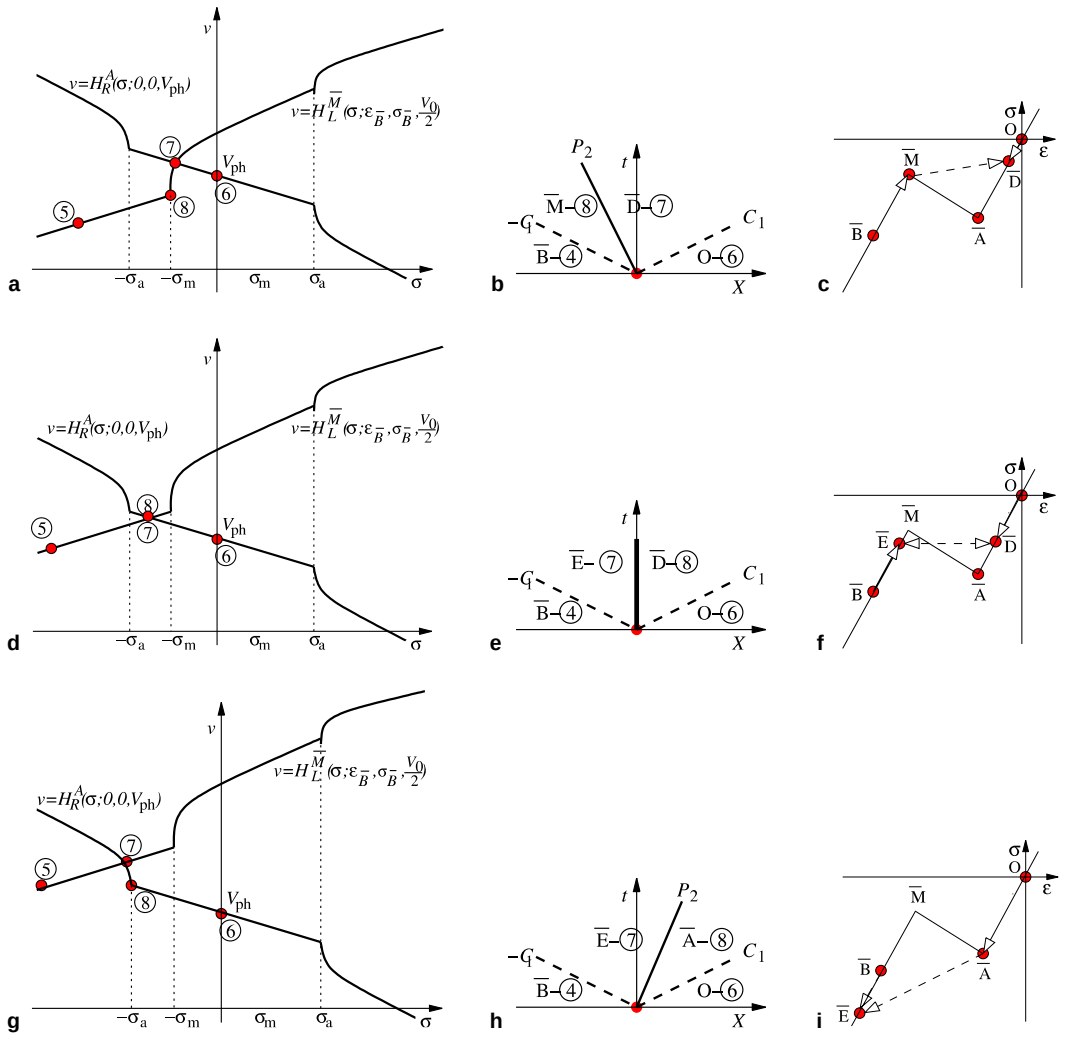

Fig. 12. Solution of the Riemann problem at point $R_2(X_2,t_2)$. Intersection of the curves $v=H_L^{\overline{M}}(\sigma;\varepsilon_{\overline{B}},\sigma_{\overline{rmB}},\frac{V_0}{2})$ and $v=H_R^A(\sigma;0,0,V_{ph})$; local space-time diagram; stress–strain states. Capital letters denote stress–strain states; encircled numbers denote stress–velocity states. {(a), (b), (c)} Case $V_0\in(V_{ph},V_{bw})$—backward propagating phase transformation. {(d), (e), (f)} Case $V_0\in[V_{bw},V_{fw}]$—stationary phase boundary $\mathscr{M}^-\leftrightarrow\mathscr{A}$. {(g), (h), (i)} Case $V_0>V_{fw}$)—forward propagating phase transformation.

respectively. While the second curve can be considered as a fixed one in the v–σ plane, the first curve depends on the impact velocity V_0 in a way which is illustrated in Fig. 12.

Let us introduce the following critical values of the impact velocity

$$V_{bw}\equiv V_{ph}+\frac{4\sigma_m(\sigma_3+2\sigma_m)}{\sqrt{\varrho E_1}(\sigma_3+4\sigma_m)}<V_{fw}\equiv V_{ph}+\frac{4\sigma_a(\sigma_3+2\sigma_a)}{\sqrt{\varrho E_1}(\sigma_3+4\sigma_a)}. \tag{36}$$

The interaction at $R_2(X_2,t_2)$ between the propagating phase boundary with the elastic unloading shock front leads to a reflected and transmitted elastic shock waves propagating with speed C_1 and to a propagating phase boundary. Depending on the magnitude of the impact velocity V_0 this phase boundary behaves as follows:

a) propagates *backward* if $V_{\rm ph} < V_0 < V_{\rm bw}$ (Fig. 12b),
b) is *stationary* if $V_{\rm bw} \leqslant V_0 \leqslant V_{\rm fw}$ (Fig. 12e),
c) propagates *forward* if $V_{\rm fw} < V_0$ (Fig. 12h).

Indeed, if $H_L^{\overline{\rm M}}(-\sigma_m;\varepsilon_{\overline{\rm B}},\sigma_{\overline{\rm B}},\frac{V_0}{2}) < H_R^A(-\sigma_m;0,0,V_{\rm ph})$, which is equivalent with $\frac{V_0}{2} - \frac{\sigma_m+\sigma_{\overline{\rm B}}(\eta)}{\sqrt{\varrho E_1}} < \frac{2\sigma_a}{\sqrt{\varrho E_1}} + \frac{\sigma_m}{\sqrt{\varrho E_1}}$, i.e. $V_0 < V_{\rm bw}$, then the two curves meet at the point (σ^*,v^*) denoted by (7), where $\sigma^* > -\sigma_m$ (Fig. 12a). Therefore, the particles which at $t = t_2$ and $X > X_2$ lay in the state O-(6) reach the state $\overline{\rm D}$-(7) due to an elastic shock wave in the phase $\mathscr{A}$. The particles which at $t = t_2$ and $X < X_2$ lay in the state $\overline{\rm B}$-(5) reach the state $\overline{\rm D}$-(7) by an elastic shock wave in the phase $\mathscr{M}^-$ and a backward propagating phase boundary (Fig. 12b).

If the impact velocity V_0 increases then the graph of the function $v = H_L^{\overline{\rm M}}(\sigma;\varepsilon_{\overline{\rm B}},\sigma_{\overline{\rm B}},\frac{V_0}{2})$ moves up. Thus, for $V_0 \geqslant V_{\rm bw}$ the graphs of the two curves, $v = H_L^{\overline{\rm M}}(\sigma;\varepsilon_{\overline{\rm B}},\sigma_{\overline{\rm B}},\frac{V_0}{2})$ and $v = H_R^A(\sigma;0,0,V_{\rm ph})$, intersect each other in their linear part so long as $H_L^{\overline{\rm M}}(-\sigma_a;\varepsilon_{\overline{\rm B}},\sigma_{\overline{\rm B}},\frac{V_0}{2}) \leqslant H_R^A(-\sigma_a;0,0,V_{\rm ph})$ (see Fig. 12d), which is equivalent with condition $V_0 \leqslant V_{\rm fw}$. The intersection point (σ^*,v^*) has the property that $\sigma^* \in (-\sigma_a,-\sigma_m)$ and as a consequence the particles in the neighborhood of $X = X_2$ will not change their phases. The solution will consist of two left and right propagating elastic shock fronts in each of the two corresponding phases, $\mathscr{M}^-$ and $\mathscr{A}$, respectively and a stationary discontinuity (Fig. 12e). This stationary discontinuity will persist so long it will not interact with another strain discontinuity.

If the impact velocity $V_0 > V_{\rm fw}$ then the solution (σ^*,v^*) will be obtained by intersecting the linear part of the curve $v = H_L^{\overline{\rm M}}(\sigma;\varepsilon_{\overline{\rm B}},\sigma_{\overline{\rm B}},\frac{V_0}{2})$ with the nonlinear part of the curve $v = H_R^A(\sigma;0,0,V_{\rm ph})$ (see Fig. 12g). In this case $\sigma^* < -\sigma_a$. Therefore the particles which initially were in the phase $\mathscr{M}^-$ will change their state due to an elastic shock front, but remaining in the same phase, while the particles which were in the phase $\mathscr{A}$ will change their phase to $\mathscr{M}^-$ by an elastic shock wave and a forward propagating phase front with speed P_2 (Fig. 12h).

Let us continue the description of the solution when at the point $R_2(X_2,t_2)$ the propagating phase boundary starts to move backward, i.e when $V_0 \in (V_{\rm ph},V_{\rm bw})$. We shall now focus on the limiting case when $V_0 \to V_{\rm ph} + 0$, (or equivalently when $\eta \to 0+$) and on its physical meaning.

In order to get the solution we have to solve Riemann problems and left Goursat problems in stress at the points marked with filled circles on Fig. 13. Besides the stress, strain and velocity states given by relations (32) and (34) which correspond to the regions shown in the time-space diagram in Fig. 13 we get the following wave structure.

At the point $R_2(X_2,t_2)$ the solution of the Riemann problem with constant left state $\overline{\rm B}$-(5) and constant right state O-(6) generates a backward propagating phase boundary separating the states

$$\overline{\rm D}\text{-}(7) \leftrightarrow \begin{cases} \varepsilon_{\overline{\rm D}}(\eta) = \frac{1}{E_1}\sigma_{\overline{\rm D}}(\eta), & \varepsilon = -\frac{1}{E_1}\frac{\sigma_m\sigma_3}{4\sigma_m+\sigma_3} \\ \sigma_{\overline{\rm D}}(\eta) = \frac{(\eta-2\sigma_m-\sigma_3)(\sqrt{\sigma_3^2+\eta^2}+\eta)+\sigma_3^2}{2[4\sigma_m+2\sigma_3-\eta-\sqrt{\sigma_3^2+\eta^2}]}, & \overset{\eta\to 0}{\to} \quad \sigma = -\frac{\sigma_m\sigma_3}{4\sigma_m+\sigma_3}, \\ v_{\overline{\rm D}}(\eta) = V_{\rm ph} - \frac{1}{\sqrt{\varrho E_1}}\sigma_{\overline{\rm D}}(\eta), & v = V_{\rm ph} + \frac{\sigma_m\sigma_3}{\sqrt{\varrho E_1(4\sigma_m+\sigma_3)}} \end{cases} \tag{37}$$

$$\overline{\rm M}\text{-}(8) \leftrightarrow \begin{cases} \varepsilon_{\overline{\rm M}}(\eta) = -\varepsilon_m, & \varepsilon = -\varepsilon_m \\ \sigma_{\overline{\rm M}}(\eta) = -\sigma_m, & \overset{\eta\to 0}{\to} \quad \sigma = -\sigma_m, \\ v_{\overline{\rm M}}(\eta) = V_{\rm ph} + \frac{\eta-2\sigma_m+\sqrt{\sigma_3^2+\eta^2}-\sigma_3}{2\sqrt{\varrho E_1}}, & v = V_{\rm ph} - \frac{\sigma_m}{\sqrt{\varrho E_1}} \end{cases} \tag{38}$$

The slope of the backward propagating phase boundary is given by

$$P_2^2(\eta) = \frac{E_1}{\varrho}\frac{\sigma_{\overline{\rm D}}(\eta)+\sigma_m}{\sigma_{\overline{\rm D}}(\eta)+E_1\varepsilon_m} < C_1^2, \overset{\eta\to 0}{\to} P_2^2(0) = \frac{E_1}{\varrho}\frac{4\sigma_m^2}{E_1\varepsilon_m(4\sigma_m+\sigma_3)-\sigma_m\sigma_3}. \tag{39}$$

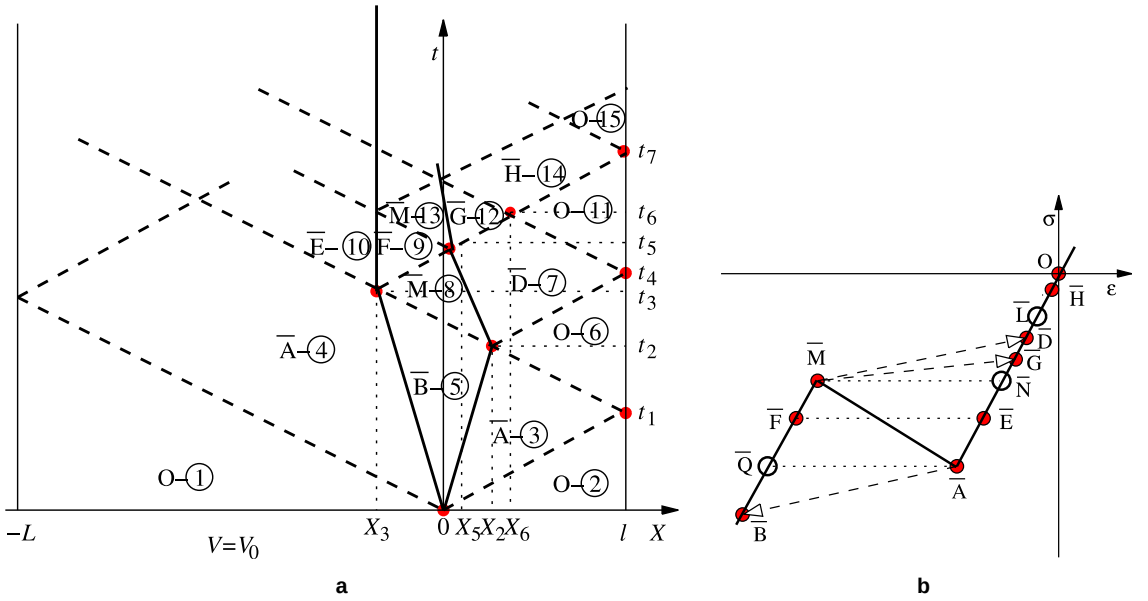

Fig. 13. Wave propagation in the flyer and target after impact—$V_0 \in (V_{\mathrm{ph}}, V_{\mathrm{bw}})$. Behavior of the backward propagating phase boundary. (a) t–X diagram, (b) stress–strain states ahead and behind discontinuities.

At the point $R_3(X_3, t_3)$ (see Fig. 13a), where the elastic unloading shock front propagating in the material lying in phase $\mathscr{M}^-$ catches up the left phase boundary, started at O(0,0), we have to solve a Riemann problem with constant left state $\overline{\mathrm{A}}$-④ and constant right state $\overline{\mathrm{M}}$- ⑧. The solution consists of two propagating left and right shock wave fronts and a stationary phase boundary which separates the constant states

$$\overline{\mathrm{F}}\text{-}⑨ \leftrightarrow \begin{cases} \varepsilon_{\overline{\mathrm{F}}}(\eta) = \frac{1}{E_1}(\sigma_{\overline{\mathrm{F}}}(\eta) - \sigma_3), & \varepsilon = -\varepsilon_m \\ \sigma_{\overline{\mathrm{F}}}(\eta) = \frac{1}{4}(\sqrt{\sigma_3^2+\eta^2} - \sigma_3 - \eta) - \sigma_m, \quad \overset{\eta\to 0}{\rightarrow} & \sigma = -\sigma_m, \\ v_{\overline{\mathrm{F}}}(\eta) = V_{\mathrm{ph}} + \frac{\sqrt{\sigma_3^2+\eta^2}-\sigma_3+3\eta-4\sigma_m}{4\sqrt{\varrho E_1}}, & v = V_{\mathrm{ph}} - \frac{\sigma_m}{\sqrt{\varrho E_1}} \end{cases} \tag{40}$$

$$\overline{\mathrm{E}}\text{-}⑩ \leftrightarrow \begin{cases} \varepsilon_{\overline{\mathrm{E}}}(\eta) = \frac{1}{E_1}\sigma_{\overline{\mathrm{E}}}(\eta), & \varepsilon = -\frac{1}{E_1}\sigma_m, \\ \sigma_{\overline{\mathrm{E}}}(\eta) = \frac{1}{4}(\sqrt{\sigma_3^2+\eta^2} - \sigma_3 - \eta) - \sigma_m, \quad \overset{\eta\to 0}{\rightarrow} & \sigma = -\sigma_m, \\ v_{\overline{\mathrm{E}}}(\eta) = V_{\mathrm{ph}} + \frac{\sqrt{\sigma_3^2+\eta^2}-\sigma_3+3\eta-4\sigma_m}{\sqrt{4\varrho E_1}}, & v = V_{\mathrm{ph}} - \frac{\sigma_m}{\sqrt{\varrho E_1}} \end{cases} \tag{41}$$

At the point $R_4(X_4 = l, t_4)$ (Fig. 13a) where the elastic loading shock wave reflected at $R_2(X_2, t_2)$ by the phase boundary reaches the free end of the target we have to solve a left Goursat problem in stress with initial condition $\overline{\mathrm{D}}$-⑦. The solution will consist of an elastic unloading shock front separating the constant states $\overline{\mathrm{D}}$-⑦ from

$$\mathrm{O}\text{-}⑪ \leftrightarrow \left(\varepsilon = 0, \sigma = 0, v = V_{\mathrm{ph}} - \frac{2\sigma_{\overline{\mathrm{D}}}(\eta)}{\sqrt{\varrho E_1}}\right) \overset{\eta\to 0}{\rightarrow} \left(\varepsilon = 0, \sigma = 0, v = V_{\mathrm{ph}} + \frac{2\sigma_m\sigma_3}{\sqrt{\varrho E_1}(4\sigma_m + \sigma_3)}\right) \tag{42}$$

At the point $R_5(X_5, t_5)$ (Fig. 13a) the forward propagating elastic shock front generated at $R_3(X_3, t_3)$ interacts with the backward propagating phase boundary. The wave structure is found by solving the Riemann problem with constant step data $\overline{\mathrm{F}}$-⑨ and $\overline{\mathrm{D}}$-⑦. We get that the phase boundary continues to propagate

backward, (but with a lower velocity, since $\sigma_{\overline{G}}(\eta) < \sigma_{\overline{D}}(\eta)$ (Fig. 13b), while the elastic shock front is reflected and transmitted across it bounding the regions with constant states

$$\overline{\mathrm{G}}\text{-}⑫ \leftrightarrow \begin{cases} \varepsilon_{\overline{G}}(\eta) = \frac{1}{E_1}\sigma_{\overline{G}}(\eta), & \varepsilon = -\frac{1}{E_1}\frac{\sigma_m\sigma_3}{4\sigma_m+\sigma_3}, \\ \sigma_{\overline{G}}(\eta) = \frac{\eta^2-2\sigma_m\eta-\sigma_m\sigma_3}{4\sigma_m+\sigma_3-2\eta}, & \overset{\eta\to 0}{\to} \quad \sigma = -\frac{\sigma_m\sigma_3}{4\sigma_m+\sigma_3}, \\ v_{\overline{G}}(\eta) = V_{\mathrm{ph}} - \frac{1}{\sqrt{\varrho E_1}}\sigma_{\overline{G}}(\eta), & v = V_{\mathrm{ph}} + \frac{\sigma_m\sigma_3}{\sqrt{\varrho E_1(4\sigma_m+\sigma_3)}} \end{cases} \tag{43}$$

$$\overline{\mathrm{M}}\text{-}⑬ \leftrightarrow \begin{cases} \varepsilon_{\overline{M}}(\eta) = -\varepsilon_m, & \varepsilon = -\varepsilon_m \\ \sigma_{\overline{M}}(\eta) = -\sigma_m, & \overset{\eta\to 0}{\to} \quad \sigma = -\sigma_m, \\ v_{\overline{M}}(\eta) = V_{\mathrm{ph}} + \frac{\eta-\sigma_m}{\sqrt{\varrho E_1}}, & v = V_{\mathrm{ph}} - \frac{\sigma_m}{\varrho E_1} \end{cases} \tag{44}$$

The unloading shock wave reflected at t_4 by the free end of the target (Fig. 13a) interacts at the point $R_6(X_6,t_6)$ with the shock wave transmitted at t_5 by the backward propagating phase boundary. Therefore, we have to solve a Riemann problem with the initial data corresponding to $\overline{\mathrm{G}}$- ⑫ and O-⑪, respectively. The solution consists of two propagating left and right shock wave fronts which are separated by the constant state

$$\overline{\mathrm{H}}\text{-}⑭ \leftrightarrow \begin{cases} \varepsilon_{\overline{H}}(\eta) = \frac{1}{E_1}(\sigma_{\overline{G}}(\eta) - \sigma_{\overline{D}}(\eta)), & \varepsilon = 0, \\ \sigma_{\overline{H}}(\eta) = \sigma_{\overline{G}}(\eta) - \sigma_{\overline{D}}(\eta), & \overset{\eta\to 0}{\to} \quad \sigma = 0, \\ v_{\overline{H}}(\eta) = V_{\mathrm{ph}} - \frac{1}{\sqrt{\varrho E_1}}(\sigma_{\overline{G}}(\eta) + \sigma_{\overline{D}}(\eta)), & v = V_{\mathrm{ph}} + \frac{2\sigma_m\sigma_3}{\sqrt{\varrho E_1(4\sigma_m+\sigma_3)}}, \end{cases} \tag{45}$$

At time $t = t_7$ (Fig. 13a) an unloading shock wave reaches again the free end of the target bar and is reflected leading to the following solution of a left Goursat problem

$$\mathrm{O}\text{-}⑮ \leftrightarrow \left(\varepsilon = 0, \sigma = 0, v = V_{\mathrm{ph}} - \frac{2\sigma_{\overline{H}}(\eta)}{\sqrt{\varrho E_1}}\right) \overset{\eta\to 0}{\to} \left(\varepsilon = 0, \sigma = 0, v = V_{\mathrm{ph}} + \frac{2\sigma_m\sigma_3}{\sqrt{\varrho E_1}(4\sigma_m+\sigma_3)}\right) \tag{46}$$

The procedure can continue in the same manner in order to determine the complete solution of our impact problem. We can now summarize the behavior of the two bars when the impact velocity is only a bit larger than the value necessary to induce a phase transformation at the impact end.

First, the unloading shock wave reflected, at the free end of the specimen, interacts successively with the right and left propagating phase boundaries changing the first one into a backward propagating phase boundary and stopping the second one. The change in acoustic impedance of the material across a phase boundary produces the reflection of elastic shock waves across it. As a consequence the presence of a transformation can be detected by recording the changes in the velocity profile at the end of the target $X = l$. According to (37) and (45), the first loading shock wave, reflected by the phase boundary at $R_2(X_2, t_2)$ induces at the free end of the target at time t_4 a significant step-like increase of the velocity. No increase in particle velocity would be expected at this moment if no phase transformations would occur. Moreover, so long as the phase boundary exists at the left end of the target any round trip propagation of the first pulse between the phase boundary and the free-end of the target will lead to a new significant increase of the particle velocity at $X = l$. On the other side, between these time moments we can also observe at $X = l$ small fluctuations of the particle velocity. These are due to the elastic shock waves propagating inside the transformed zone and which are transmitted across the phase boundary.

Let us analyze now the limit case when $V_0 \to V_{\mathrm{ph}}$, $V_0 > V_{\mathrm{ph}}$, i.e. $\eta \to 0$, $\eta > 0$. The behavior of the solution, illustrated in Fig. 14, is obtained by collecting the results described in relations (32)–(46) for $\eta \to 0$. The elastic model, coupled with the chord criterion, predicts that as soon as the impact velocity overcomes the critical value V_{ph}, a phase boundary starts to propagate in both bars. When $\eta \to 0$ the speed of the

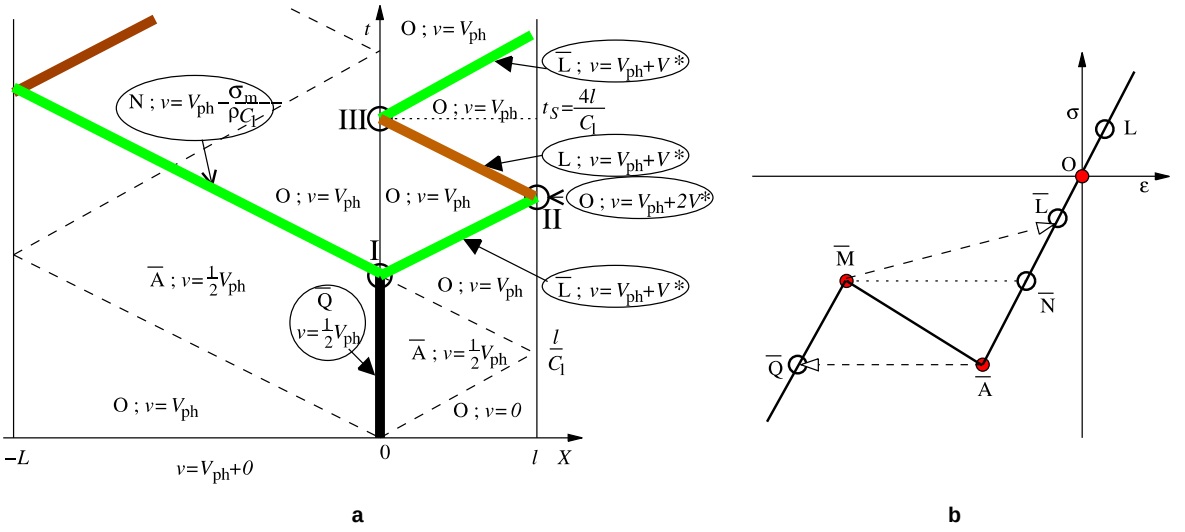

Fig. 14. Wave propagation in the flyer and target after impact. The limit case $V_0 = V_{ph} + 0$. (a) t–X diagram, (b) stress–strain states ahead and behind discontinuities.

phase boundary is going to zero and the strain-stress state of the transformed material is going to $\overline{Q}(-\frac{1}{E_1}(\sigma_a+\sigma_3), -\sigma_a)$ (see Fig. 14b). In other words, according to (32), the slope of the straight line connecting the nucleation strain-stress state $\overline{A}(-\varepsilon_a, -\sigma_a)$ and the transformed strain-stress state $\overline{B}(-\varepsilon_{\overline{B}}, -\sigma_{\overline{B}})$ becomes horizontal.

At the time t_2 when the unloading shock wave reflected at the free end of the target starts to cross the transformed material the thickness of the transformed zone is of the order of $\eta(X_2 - X_3 = \frac{2l}{\sigma_3}\eta)$. At this moment a reverse phase transformation $\mathscr{M}^- \to \mathscr{A}$, starts to develop and a backward propagating phase boundary starts to advance into material lying in the $\mathscr{M}^-$ phase. It is interesting to note that, according to (39), the reverse transformation can not propagate faster than a limit speed value given by $P_2(0)$. This corresponds to the straight line connecting the states $\overline{M}(-\varepsilon_m, -\sigma_m)$ and $\overline{L}(-\frac{1}{E_1}\frac{\sigma_m\sigma_3}{4\sigma_m+\sigma_3}, -\frac{\sigma_m\sigma_3}{4\sigma_m+\sigma_3})$ (Fig. 14b).

We are interested to determine what happens when the backward propagating phase boundary in the target interacts with the stationary phase boundary generated in the flyer. It is obvious that, when $\eta \to 0$, we can assume that the backward propagating phase boundary moves with the constant speed $P_2(0) < 0$, and using relations (41) and (43) we can approximate the solution at the left of the intersection point of the two phase boundaries by the constant strain-stress state $\overline{N}(-\frac{\sigma_m}{E_1}, -\sigma_m)$ and velocity $v = V_{ph} - \frac{1}{\varrho C_1}\sigma_m$ and at the right of the intersection point by the constant compressive strain-stress state $\overline{L}(-\frac{1}{E_1}\frac{\sigma_m\sigma_3}{4\sigma_m+\sigma_3}, -\frac{\sigma_m\sigma_3}{4\sigma_m+\sigma_3})$ and velocity $v = V_{ph} + V^*$ (see point I in Fig. 14a and its zoom in Fig. 15a) where

$$V^* = \frac{1}{\sqrt{\varrho E_1}}\frac{\sigma_m\sigma_3}{4\sigma_m+\sigma_3}. \tag{47}$$

The solution of the above Riemann problem will consist in two *unloading* elastic shock waves propagating left and right, respectively and bounding a region in the time-space diagram where

$$\varepsilon = 0,\ \sigma = 0,\ v = V_{ph}. \tag{48}$$

Therefore, around the time $t \approx \frac{2l}{C_1}$, which corresponds to a round trip through the thickness of the target of the initial pulse, two parallel shock waves discontinuities very close each other are generated near the contact point (Fig. 15a). The first one propagating right is a *loading* shock and is due to the interaction between

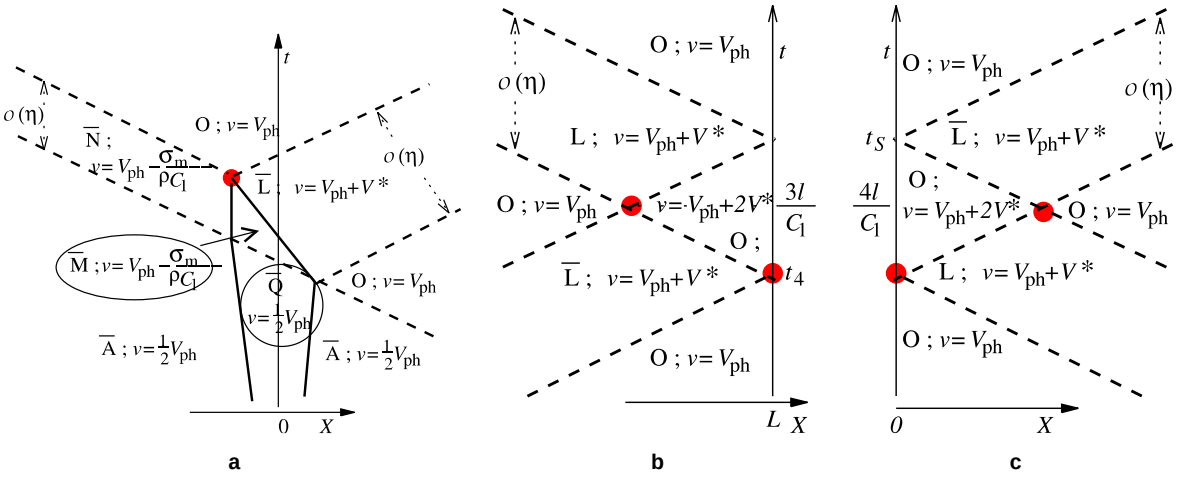

Fig. 15. The limit case $V_0 = V_{ph} + 0$. (a) Zoom of zone I in Fig. 14a. Interaction between backward propagating phase boundary and the stationary phase boundary. (b) Zoom of zone II in Fig. 14a. Reflection of the "elastic pulse" at the free end of the target bar. (c) Zoom of zone III in Fig. 14a. Reflection of the "elastic pulse" at the impact end of the target bar. Capital letters denote stress–strain states in Fig. 14b.

the first elastic pulse with the phase boundary, while the second one propagating also right is an *unloading* shock wave and is due to the interaction between the two phase boundaries which disappear. These two shock fronts form in the space time diagram a narrow strip whose order of magnitude is proportional with η. Inside this strip we have the compressive strain-stress state $\overline{L}$.

The above two discontinuities arrive at the free end of the target at a time $t \approx \frac{3l}{C_1}$ (point II in Fig. 14a) and the solution corresponding to this interaction is determined by solving Riemann and Goursat problems at the point marked with filled circles in its zoom in Fig. 15b. Therefore, an infinitesimal transformed zone induced by impact at the left end of the target leads to an unusual increase of the particle velocity at the free end of the specimen. This will be recorded like a small pulse of the velocity for a time interval proportional with η. The two shock discontinuities are reflected by the boundary $X = l$. The first one will arrive at the left end of the target $X = 0$ (point III in Fig. 14a) as a *tensile wave* (the strain-stress state inside the strip propagating now left is positive, i.e. $L\left(\frac{1}{E_1}\frac{\sigma_m\sigma_3}{4\sigma_m+\sigma_3}, \frac{\sigma_m\sigma_3}{4\sigma_m+\sigma_3}\right)$ in Fig. 14b), leading to the separation of the two bars. Thus, the time of separation is around $t_S = \frac{4l}{C_1}$. The way these shock discontinuities are reflected by the left end of the target is illustrated in Fig. 15c where the solution is determined by solving Riemann and Goursat problems at the points marked with filled circles.

Therefore, another indication of the existence of a phase boundary at the impact face is an abrupt change of the time of separation of the two bars. Indeed, according to the above bar theory when the projectile is longer than the target bar and $E_1 = E_3$, the separation of the two bars should appear, at time $t = \frac{2L}{C_1}$ if the contact is elastic, i.e. when $V_0 \leqslant V_{ph}$, and at time $t = \frac{4l}{C_1}$ when $V_0 = V_{ph} + 0$ and an infinitesimal part of the impact region suffers a phase transformation. Thus, an experimental investigation on the influence of the impact velocity on the time of separation could clarify some aspects connected with the dynamic nucleation of phases.

Another indication of the existence of a phase boundary at the impact face is the periodic increase of the particle velocity at the free end of the target which is associated with the arrivals of the elastic pulses at this border (see for instance Fig. 16). This result is in agreement with experimental observations as those performed by Escobar and Clifton (1995).

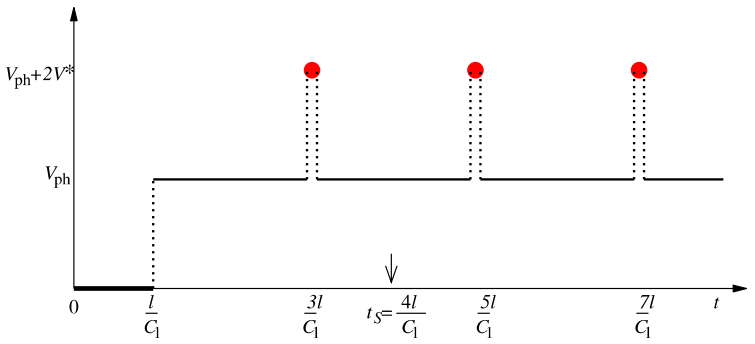

Fig. 16. The limit case $V_0 = V_{ph} + 0$. Effect of phase transformation: changes in the free-end velocity of the target bar associated with the arrivals of the elastic waves.

6. Summary and concluding remarks

The aim of this study is to provide a complete theoretical and numerical analysis on the wave structure predicted by the elastic model versus a general rate-type viscoelastic approach when we consider the longitudinal impact of two phase transforming bars. This analysis allows, on one side, a qualitatively and quantitatively comparison between the solutions described by the two models and, on the other side, give suggestions on the way these results can be used to interpret laboratory experiments.

In this first part, by using a piecewise linear non-monotone elastic constitutive equation we investigated solutions for the complete set of Riemann and Goursat problems. The non-uniqueness issue inherent to such problems due to the non-convexity of the free energy function was eliminated by using the chord criterion which, according to Part II (Făciu and Molinari, 2005), is furnished by our augmented theory. By using systematically the solutions of the Goursat and Riemann problems we started to build the exact solution for a variety of impact conditions. We explored the interaction between elastic shock waves transmitted and reflected across phase boundaries. We found *critical values of the impact velocity* such that the impact-induced phase boundary continues to move forward after its interaction with an unloading elastic wave, or comes to rest, or starts to move down the bar. We focus on the effect of these interactions on the variation of the particle velocity at the free end of the target.

We studied in much more details the limiting case when the impact velocity overcomes a nucleation value. Interaction between the phase boundaries induced in the target and flyer in this case is investigated. We derived that a direct consequence of this event is a sudden drop of the time of separation between the two bars after their contact. This behavior is easily to be tested experimentally and can offer some insight on the stress required for $\mathscr{A} \leftrightarrow \mathscr{M}\pm$ phase transformation.

The solutions of the Riemann and Goursat problems derived here can also be used to built numerical schemes of Godunov type (see LeVeque, 1990) for the elastic system of conservation law.

The first natural continuation of this paper is the investigation of the wave structure predicted by the Maxwellian rate-type model when considering the same impact problem. The analysis of the similarities and differences between the two approaches is investigated in Part II (Făciu and Molinari, 2005). The second one concerns the modeling of thermal aspects accompanying the impact-induced phase transformation which will be done in a future work.

Acknowledgements

The authors acknowledge partial support of the EURROMMAT Programme ICA1-CT 2000-70022 of the European Commission. C.F. also acknowledge support from the Romanian Ministry of Education and

Research (CERES Programme Project 4-187/2004). C.F. is grateful for the warm hospitality of the University of Metz during his research stays at LPMM.

References

Abeyaratne, R., Knowles, J.K., 1991a. Kinetic relations and the propagation of phase boundaries in solids. Arch. Rational Mech. Anal. 114, 119–154.

Abeyaratne, R., Knowles, J.K., 1991b. Implications of viscosity and strain-gradient effects for the kinetics of propagating phase boundaries in solids. SIAM J. Appl. Math. 51, 1205–1221.

Abeyaratne, R., Knowles, J.K., 1993. A continuum model of a thermoelastic solid capable of undergoing phase transitions. J. Mech. Phys. Solids 41, 541–571.

Bell, J.F., 1968. The Experimental Foundations of Solid Mechanics. Handbuch der Physik, Vol. VIa/1. Springer-Verlag, Berlin–Heidelberg–New York.

Bruno, O., Vaynblat, D., 2001. Shock-induced martensitic phase transitions: Critical stresses, Riemann problems and applications. Proc. R. Soc. Lond. A 457, 2871–2920.

Chen, Y.-C., Lagoudas, D.C., 2000. Impact induced phase transformation in shape memory alloys. J. Mech. Phys. Solids 48, 275–300.

Cristescu, N., Suliciu, I., 1982. Viscoplasticity. Martinus Nijhoff Publishers, The Hague/Boston/London.

Dafermos, C.M., 1973. The entropy rate admissibility criterion for solutions of hyperbolic conservation laws. J. Differ Equat 14, 202–212.

Ericksen, J.L., 1975. Equilibrium of bars. J. Elast 5, 191–201.

Escobar, J.C., Clifton, R.J., 1995. Stress-wave induced martensitic phase transformations. In: Murr, L.E., Staudhammer, K.P., Meyers, M.A. (Eds.), Metallurgical and Materials Applications of Shock-Wave and High-Strain-Rate Phenomena. Elsevier Science B.V., pp. 451–462.

Făciu, C., 1996. Initiation and growth of strain bands in rate-type viscoelastic materials. Part I: Discontinuous strain solutions. Part II: The energetics of the banding mechanism. European J. Mech. A/Solids 15, 969–988, 989–1011.

Făciu, C., Mihăilescu-Suliciu, M., 1987. The energy in one dimensional rate-type semilinear viscoelasticity. Int. J. Solids Struct. 11, 1505–1520.

Făciu, C., Mihăilescu-Suliciu, M., 2002. On modelling phase propagation in SMAs by a Maxwellian thermo-viscoelastic approach. Int. J. Solids Struct. 39, 3811–3830.

Făciu, C., Molinari, A., 2005. On the longitudinal impact of two phase transforming bars. Elastic versus a rate-type approach. Part II: The rate-type case. Int. J. Solids Struct., in press, doi:10.1016/j.ijsolstr.2005.06.022.

Făciu, C., Suliciu, I., 1994. A Maxwellian model for pseudoelastic materials. Scripta Metall. Mater. 31, 1399–1404.

Hattori, H., 1986. The Riemann problem for a van der Waals fluid with entropy rate admissibility criterion—isothermal case. Arch. Rational Mech. Anal. 92, 247–263.

James, R.D., 1980. The propagation of phase boundaries in elastic bars. Arch. Rational Mech. Anal. 73, 125–158.

James, R.D., 1981. Finite deformation by mechanical twinning. Arch. Rational Mech. Anal. 77, 143–176.

Lagoudas, D.C., Ravi-Chandar, K., Sarh, K., Popov, P., 2003. Dynamic loading of polycrystalline shape memory alloy rods. Mech. Mater. 35, 689–716.

Lax, P.D., 1971. Shock waves and entropy. In: Zarantonello, E.A. (Ed.), Contributions to Nonlinear Functional Analysis. Academic Press, NY, pp. 603–634.

LeVeque, R.J., 1990. Numerical Methods for Conservation Laws. Birkhäuser-Verlag, Basel.

Ngan, S.-C., Truskinovsky, L., 2002. Thermo-elastic aspects of dynamic nucleation. J. Mech. Phys. Solids 50, 1193–1229.

Otsuka, K., Wayman, C.M., Nakai, K., Sakamoto, H., Shimizu, K., 1976. Superelasticity effects and stress-induced martensitic transformations in Cu–Al–Ni alloys. Acta Metall. 24, 207–226.

Pego, R.L., 1987. Phase transitions in one-dimensional nonlinear viscoelasticity: Admissibility and stability. Arch. Rational Mech. Anal. 97, 353–394.

Pence, T.J., 1992. On the mechanical dissipation of solutions to the Riemann problem for impact involving a two-phase elastic material. Arch. Rational Mech. Anal. 117, 1–52.

Shaw, J.A., Kyriakides, S., 1997. On the nucleation and propagation of phase transformation fronts in a NiTi alloy. Acta Mater. 45, 683–700.

Slemrod, M., 1983. Admissibility criteria for propagating phase boundaries in a van der Waals fluid. Arch. Rational Mech. Anal. 81, 301–315.

Suliciu, I., 1989a. Riemann and Goursat step data problems for fluids of van der Waals type. Rev. Roum. Mathé. Pures et Appl. 34, 561–572.

Suliciu, I., 1989b. On the description of the dynamics of phase transitions by means of rate-type constitutive equation. A model problem. In: Khan, A.S.K., Tokuda, M. (Eds.), Proceedings of Plasticity '89. Pergamon Press, pp. 417–420.

Suliciu, I., 1990. On modeling phase transitions by means of rate-type constitutive equations. Shock wave structure. Int. J. Eng. Sci. 28, 829–841.

Suliciu, I., 1992. Some stability-instability problems in phase transitions modeled by piecewise linear elastic or viscoelastic constitutive equations. Int. J. Eng. Sci. 30, 483–494.

Truskinovsky, L., 1985. Structure of isothermal phase jump. Sov. Phys. Doklady 30, 945–948.

Truskinovsky, L., 1987. Dynamics of nonequilibrium phase boundaries in a heat conducting nonlinear elastic medium. J. Appl. Math. (PMM) 51, 777–784.

Vainchtein, A., Rosakis, P., 1999. Hysteresis and stick-slip motion of phase boundaries in dynamic models of phase transitions. J. Nonlinear Sci. 9, 697–719.